Cellular plasticity of the bone marrow niche promotes hematopoietic stem cell regeneration

Hiroyuki Hirakawa[1,2], Longfei Gao[1,2], Daniel Naveed Tavakol[1,3], Gordana Vunjak-Novakovic[1,3,4] & Lei Ding [1,2] ✉

Hematopoietic stem cells (HSCs) regenerate after myeloablation, a procedure that adversely disrupts the bone marrow and drives leptin receptor-expressing cells, a key niche component, to differentiate extensively into adipocytes. Regeneration of the bone marrow niche is associated with the resolution of adipocytes, but the mechanisms remain poorly understood. Using *Plin1-creER* knock-in mice, we followed the fate of adipocytes in the regenerating niche in vivo. We found that bone marrow adipocytes were highly dynamic and dedifferentiated to leptin receptor-expressing cells during regeneration after myeloablation. Bone marrow adipocytes could give rise to osteolineage cells after skeletal injury. The cellular fate of steady-state bone marrow adipocytes was also plastic. Deletion of adipose triglyceride lipase (*Atgl*) from bone marrow stromal cells, including adipocytes, obstructed adipocyte dedifferentiation and led to severely compromised regeneration of HSCs as well as impaired B lymphopoiesis after myeloablation, but not in the steady state. Thus, the regeneration of HSCs and their niche depends on the cellular plasticity of bone marrow adipocytes.

HSCs are maintained by the bone marrow niche, of which leptin receptor-expressing (LepR+) stromal cells are a key component[1–5]. These cells serve as the major source of *Scf*, *Cxcl12* and *Il7* to support HSCs and hematopoiesis in the bone marrow[1,2,6,7]. LepR+ cells are of mesenchymal origin, expressing full-length LepR protein and the marker profile CD45/Ter119/CD31-PDGFRα+. These cells are precursors to bone marrow adipocytes and also give rise to bone in adults[8,9]. Recent single-cell RNA sequencing (scRNA-seq) data showed considerable heterogeneity within LepR+ cells, because some express osteogenic genes, whereas others express adipogenic genes[10–13]. Although the adipolineage-committed LepR+ mesenchymal progenitor subset labeled by *Cxcl12-creER* can differentiate into osteoblasts after bone injury[14], it is not clear whether terminally differentiated mesenchymal cells of one lineage can alter their fate to become cells of a different lineage in bone marrow.

The niche is also critical for HSC and hematopoietic regeneration after myeloablation, a prerequisite for successful HSC transplantation. Besides deleterious effects on the hematopoietic compartment, myeloablation drastically disrupts the bone marrow stroma. The sinusoids become dilated and leaky as the bone marrow becomes hypocellular[8,15,16]. In parallel, the number of LepR+ cells declines and excessive adipocytes fill up the bone marrow[17]. The niche then needs to be regenerated for the recovery of HSCs and hematopoiesis[8,15,16,18]; however, it is poorly understood how adipocytes contract to give way to hematopoiesis, and how LepR+ cells, central components of the bone marrow HSC niche, regenerate after myeloablation.

[1]Columbia Stem Cell Initiative, New York, NY, USA. [2]Department of Rehabilitation and Regenerative Medicine, Department of Microbiology and Immunology, Columbia University Irving Medical Center, New York, NY, USA. [3]Department of Biomedical Engineering, Columbia University, New York, NY, USA. [4]Department of Medicine, Columbia University, New York, NY, USA. ✉e-mail: ld2567@cumc.columbia.edu
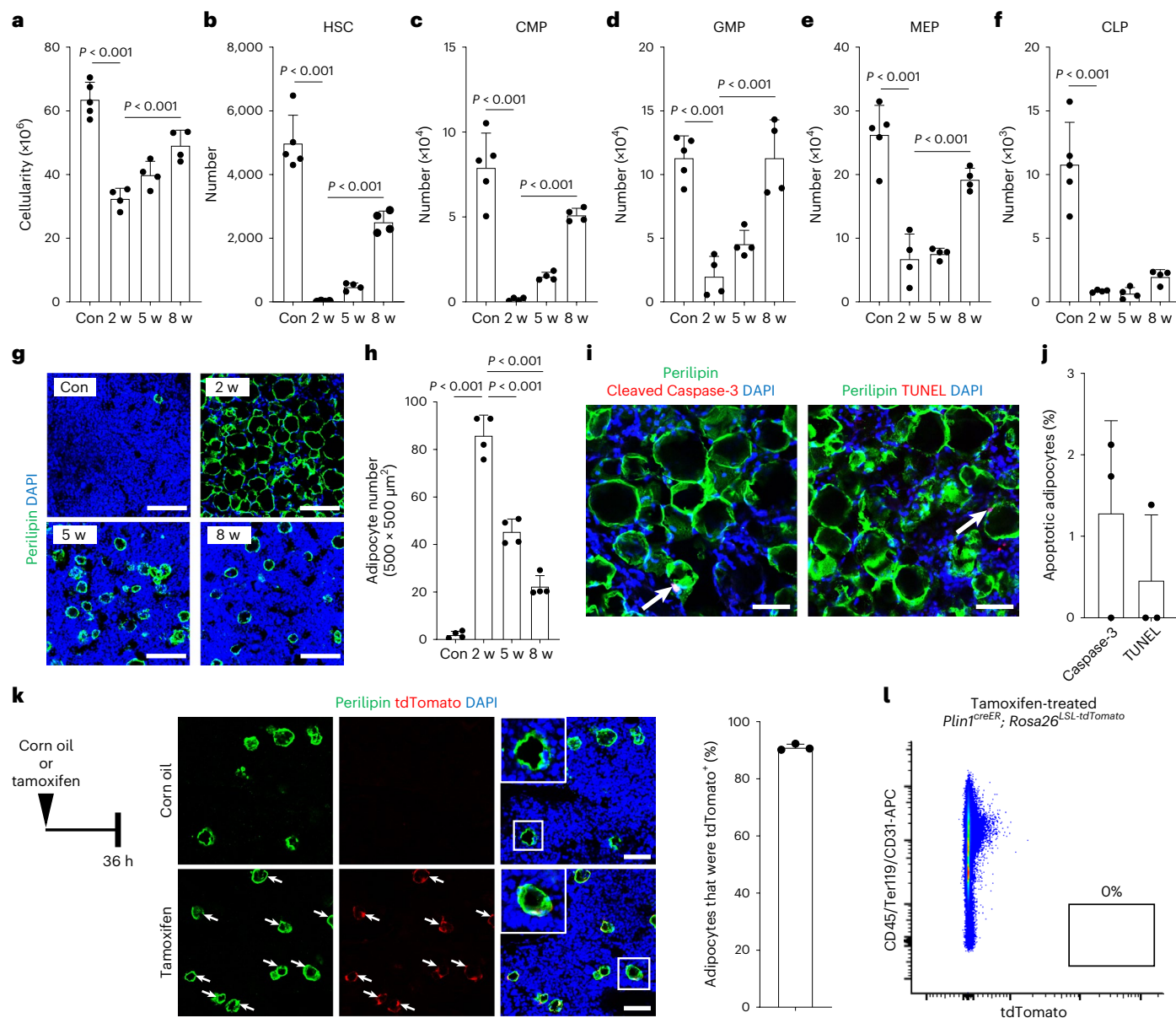
Fig. 1 | Expanded adipocytes contract in parallel with bone marrow regeneration after irradiation. a–h, Bone marrow from sublethally irradiated (6 Gy) wild-type mice was analyzed at 2, 5 and 8 weeks (2, 5 and 8 w) postirradiation. Nonirradiated mice were analyzed as controls (Con). Numbers of whole bone marrow (**a**), HSC (**b**), CMP (**c**), GMP (**d**), MEP (**e**) and CLP (**f**) cells ($n = 5$ for Con, $n = 4$ for 2, 5 and 8 weeks, one femur and one tibia were used for analysis) are shown. Representative images (**g**) and quantification (**h**) of irradiation-induced bone marrow adipocytes (stained with an anti-perilipin antibody) ($n = 4$ for each group). **i,j,** Representative images (**i**) and quantification of apoptotic adipocytes (**j**) ($n = 3$) in the bone marrow at 2 weeks postirradiation.

k, Experimental scheme, representative whole-mount confocal images and quantification of bone marrow perilipin+ adipocytes that were tdTomato+ ($n = 3$) from *Plin1*^{creER}; *Rosa26*$^{LSL-tdTomato}$ mice 36 h after tamoxifen administration. Adipocytes were stained with an anti-perilipin antibody (in green). Arrows point to tdTomato+ adipocytes. Squares indicate enlarged regions. **l,** Representative flow cytometry plot showing no detectable tdTomato+ cells in enzymatically digested bone marrow cells from *Plin1*^{creER}; *Rosa26*$^{LSL-tdTomato}$ mice 36 h after tamoxifen administration ($n = 3$). All data represent mean ± s.d. One-way analysis of variance (ANOVA) followed by Dunnett's test was used to assess statistical significance. Scale bar, 100 μm.

Results

Dynamics of bone marrow adipocyte number after irradiation

Because adipocytes are the predominant stromal cells in the bone marrow after myeloablation[17], we assess adipocyte dynamics associated with hematopoietic regeneration in sublethally irradiated wild-type mice. Bone marrow myeloid and megakaryocytic cells were quickly depleted, whereas erythroid cells increased significantly at 2 weeks postirradiation (Extended Data Fig. 1a–j). By 8 weeks, these hematopoietic parameters mostly returned to baseline levels (Extended Data Fig. 1a–j). Bone marrow cellularity and restricted hematopoietic progenitors, including

common myeloid progenitors (CMPs), granulocyte/macrophage progenitors (GMPs) and megakaryocytic/erythroid progenitors (MEPs), were significantly depleted at 2 weeks but largely recovered by 8 weeks postirradiation, whereas HSCs and common lymphoid progenitors (CLPs) gradually regenerated at slower kinetics (Fig. 1a–f). Along with the depletion and subsequent regeneration of the bone marrow hematopoiesis, large numbers of perilipin+ adipocytes accumulated and then decreased between 2 and 8 weeks postirradiation (Fig. 1g,h). A negligible portion of adipocytes was positive for cleaved caspase-3 or TUNEL at 2 weeks postirradiation (Fig. 1i,j). The lack of extensive cell death

suggests that adipocyte number may decline through mechanisms other than apoptosis during bone marrow regeneration.

Labeling and tracing of bone marrow adipocytes in vivo

To follow the fate of adipocytes, we searched for markers that specifically label adipocytes in the bone marrow. We examined recently published scRNA-seq datasets on bone marrow stroma[11,12]. Because mature adipocytes are too large and fragile to capture using flow cytometry or scRNA-seq[19,20], these datasets do not include adipocytes. Although adiponectin (*Adipoq*) has been used as a marker for adipocytes, its expression mirrored that of *Lepr* in the bone marrow, suggesting that adiponectin marks LepR^{+} cells (Extended Data Fig. 2a–d). However, *Plin1*, a marker for mature adipocytes, was not expressed by mesenchymal stromal cells or hematopoietic cells in the bone marrow (Extended Data Fig. 2a–d). In line with the scRNA-seq data, PCR with reverse transcription (RT–PCR) analysis confirmed that *Plin1* was expressed by adipocytes, but not CD45/Ter119/CD31^{−}PDGFRα^{+} bone marrow mesenchymal stromal cells (Extended Data Fig. 2e). We generated *Plin1*[creER] knock-in mice by inserting a *P2A-creER* cassette into the locus of *Plin1* (Extended Data Fig. 2f,g), allowing expression of *creER* under the control of the endogenous *Plin1* promoter without compromising *Plin1* expression. Indeed, *Plin1*[creER/creER] homozygous mice were normal and expressed perilipin protein in the bone marrow (Extended Data Fig. 2g,h).

We then generated *Plin1*[creER/+]; *Rosa26*[LSL-tdTomato] mice. The metaphyses of 2-month-old young adult *Plin1*[creER/+]; *Rosa26*[LSL-tdTomato] mice were analyzed by whole-mount confocal microscopy 36 h after one dose of tamoxifen treatment. Corn oil-treated control *Plin1*[creER/+]; *Rosa26*[LSL-tdTomato] mice had no tdTomato^{+} cells in the bone marrow. Strikingly, 90% of perilipin[+] mature adipocytes, but not any other cells, were labeled with tdTomato in the bone marrow of tamoxifen-treated *Plin1*[creER/+]; *Rosa26*[LSL-tdTomato] mice (Fig. 1k). Consistently, flow cytometry analysis, which cannot capture mature adipocytes, revealed that tamoxifen-treated *Plin1*[creER/+]; *Rosa26*[LSL-tdTomato] mice had no tdTomato^{+} cells in the bone marrow, confirming that *Plin1-creER* does not label any cells other than mature adipocytes in the bone marrow (Fig. 1l).

Bone marrow adipocytes dedifferentiate to LepR^{+} cells

We sublethally irradiated *Plin1*[creER/+]; *Rosa26*[LSL-tdTomato] mice and administered three doses of tamoxifen on alternating days starting on day 10 after irradiation. The number of bone marrow adipocytes was not altered by tamoxifen treatment (Extended Data Fig. 2i–k). One day after administration of the final dose of tamoxifen, virtually all mature bone marrow perilipin[+] adipocytes were expressing tdTomato (Extended Data Fig. 2l). These data suggest that bone marrow adipocytes are efficiently labeled by *Plin1-creER* after myeloablation.

We irradiated *Plin1*[creER/+]; *Rosa26*[LSL-tdTomato] mice, administered three doses of tamoxifen on days 10, 12 and 14 after irradiation, and followed the fate of adipocytes during bone marrow regeneration (Fig. 2a). We analyzed the mice at 5 and 8 weeks postirradiation when the number

of bone marrow adipocytes significantly decreases (Fig. 1g,h). Flow cytometry analysis of enzymatically disassociated bone marrow cells revealed a 26-fold increase in the frequency and a 43-fold increase in the number of tdTomato^{+} cells from *Plin1*[creER/+]; *Rosa26*[LSL-tdTomato] mice analyzed at 8 weeks postirradiation compared with 15 days postirradiation (Fig. 2b).

Because adipocytes are refractory to flow cytometry analysis (Fig. 1l and ref. 20), we wondered about the identity of the adipocyte-derived tdTomato^{+} cells captured by flow cytometry. In line with wild-type mice (Fig. 1g,h), whole-mount confocal microscopic analyses showed that the number of mature perilipin[+] adipocytes in the bone marrow from tamoxifen-treated *Plin1*[creER/+]; *Rosa26*[LSL-tdTomato] mice markedly decreased over time between 2 and 8 weeks postirradiation (Fig. 2c and Extended Data Fig. 2m). Interestingly, a substantial portion of tdTomato^{+} cells neither exhibited large round mature adipocyte morphology nor expressed the mature adipocyte marker perilipin (Fig. 2c). Instead, these tdTomato^{+} cells assumed a stromal morphology with extensive cellular processes (Fig. 2c). The portion of tdTomato[+] adipocyte-derived stromal cells (perilipin[−]) increased from 52% at 5 weeks to 79% at 8 weeks postirradiation (Fig. 2d). Taken together, these data suggest that mature adipocytes gradually assume a stromal cell fate during bone marrow regeneration following irradiation.

The morphology of the tdTomato^{+} stromal cells resembled that of LepR^{+} cells. Immunostaining demonstrated that the tdTomato^{+} stromal cells were indeed expressing LepR (Fig. 2e,f). Because LepR^{+} cells are uniformly PDGFRα[+] (ref. 8), we further generated *Plin1*[creER/+]; *Rosa26*[LSL-tdTomato]; *Pdgfrα*[GFP/+] mice. Flow cytometric analyses showed that about 98% of tdTomato^{+} stromal cells were *Pdgfrα*-GFP[+] (Fig. 2g). Corroborating these results, confocal microscopic analyses showed that adipocyte-derived tdTomato^{+} cells were *Pdgfrα*-GFP[+] with a typical perivascular mesenchymal stromal cell arrangement (Fig. 2h). Thirty percent of *Pdgfrα*-GFP^{+} stromal cells were tdTomato[+] (Fig. 2h), suggesting that a substantial portion of bone marrow mesenchymal stromal cells were derived from adipocytes following irradiation. Considering that LepR^{+} cells differentiate into mature adipocytes[8], these data suggest that bone marrow adipocytes dedifferentiate to LepR[+] mesenchymal stromal cells during bone marrow regeneration.

Quantitative PCR with reverse transcription (RT–qPCR) analyses demonstrated that sorted adipocyte-derived tdTomato^{+} stromal cells expressed significantly lower levels of the adipocyte markers *Plin1* and *Fabp4* compared with bone marrow adipocytes (Fig. 2i). Relative to bone marrow adipocytes at 15 days postirradiation, adipocyte-derived tdTomato^{+} stromal cells expressed significantly higher levels of *Scf*, *Cxcl12* and *Il7*, markers for LepR[+] mesenchymal stromal cells and key cytokines for HSCs and hematopoiesis (Fig. 2j). The levels of these niche factors in adipocyte-derived tdTomato^{+} stromal cells were largely comparable with those in steady-state bone marrow LepR^{+} cells (sorted by the CD45/Ter119/CD31^{−}PDGFRα^{+} marker profile) (Fig. 2j). The adipocyte-derived tdTomato^{+} stromal cells also expressed interleukin-7

**Fig. 2 | Bone marrow adipocytes dedifferentiate to mesenchymal stromal cells during bone marrow regeneration after irradiation. a**, Experimental scheme. *Plin1*[creER]; *Rosa26*[LSL-tdTomato] mice were sublethally irradiated, treated with tamoxifen and analyzed at the indicated time. **b**, Flow cytometric quantification of the frequency and number of tdTomato^{+} cells in the tibia from *Plin1*[creER]; *Rosa26*[LSL-tdTomato] mice at 15 days (*n* = 3) and 8 weeks (*n* = 7) postirradiation. **c,d**, Representative images (**c**) and frequency of tdTomato^{+} cells that were perilipin[−] (**d**) (*n* = 3 for each group) in the bone marrow. **e,f**, Representative bone marrow images at the steady state (**e**) and 8 weeks postirradiation (**f**) (*n* = 3). LepR was stained with an antibody (in green). Arrows indicate tdTomato[+]LepR^{+} cells. **g,h**, *Plin1*[creER]; *Rosa26*[LSL-tdTomato]; *Pdgfrα*[GFP/+] mice were treated as in **a** and analyzed at 8 weeks postirradiation. GFP, green fluorescent protein. Flow cytometric plots show that nearly all adipocyte-derived tdTomato^{+} cells were *Pdgfrα*-GFP[+] (**g**) (*n* = 3). Representative image and quantification of *Pdgfrα*-GFP^{+} cells that were tdTomato[+] in the bone marrow (**h**) (*n* = 3). Arrows

indicate tdTomato[+]*Pdgfrα*-GFP^{+} cells. **i,j**, Expression levels of markers of adipocytes (*Plin1* and *Fabp4*) (**i**) and mesenchymal stromal cells (*Scf*, *Cxcl12* and *Il7*) (**j**) in tdTomato^{+} cells from *Plin1*[creER]; *Rosa26*[LSL-tdTomato] mice at 8 weeks postirradiation (tamoxifen administration as in **a**). Adipo, enriched steady-state bone marrow adipocytes (*n* = 4); LepR^{+}, LepR^{+} (CD45/Ter119/CD31^{−}PDGFRα^{+}) bone marrow mesenchymal stromal cells (*n* = 4); 15 d adipo, enriched bone marrow adipocytes at 15 days postirradiation (*n* = 3); 8 w tdT, tdTomato^{+} stromal cells at 8 weeks postirradiation (*n* = 4). All cells were sorted except adipocytes, which were enriched (Methods). ND, not detected. **k,l**, Representative images (**k**) (*n* = 2) and flow cytometric plots (**l**) (*n* = 3) showing that bone marrow adipocyte-derived stromal cells expressed IL-7 and CXCL12 at 8 weeks postirradiation in *Plin1*[creER]; *Rosa26*[LSL-tdTomato] mice. Arrows indicate tdTomato[+]IL-7^{+} cells in **k**. All data represent mean ± s.d. Two-sided Student's *t*-tests were used in **b** and **i** (*Plin1*). One-way ANOVAs followed by Bonferroni post hoc comparison tests were used in **d**, **i** (*Fabp4*) and **j**. Scale bar, 100 μm (**c**), 50 μm (**e,f,h,k**). Squares indicate enlarged regions in **h** and **k**.

(IL-7) and CXCL12 proteins (Fig. 2k,l). These data strengthen the notion that adipocytes dedifferentiate to LepR⁺ stromal cells during bone marrow regeneration after irradiation.

To control for the possible toxicity of high-dose tamoxifen on lineage tracing[21,22], we administered a single low dose of tamoxifen (0.2 mg) to sublethally irradiated $Plin1^{creER/+}; Rosa26^{LSL-tdTomato}$ mice at 14 days postirradiation (Extended Data Fig. 3a). Thirty-six hours later, whole-mount microscopic analysis revealed that about 32% of perilipin⁺ mature bone marrow adipocytes, but not any other cells, were labeled with tdTomato (Extended Data Fig. 3b,c). Flow cytometry analysis
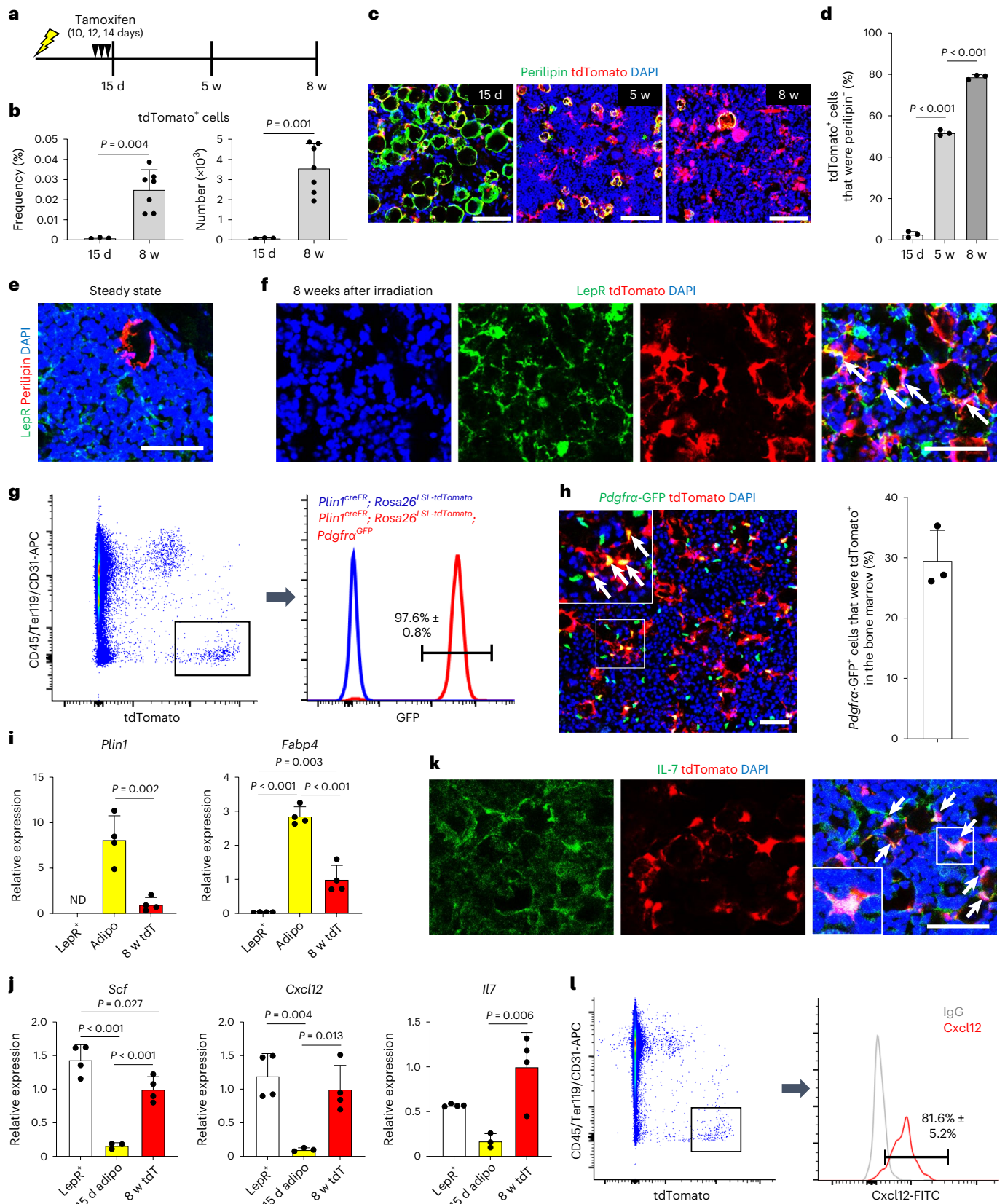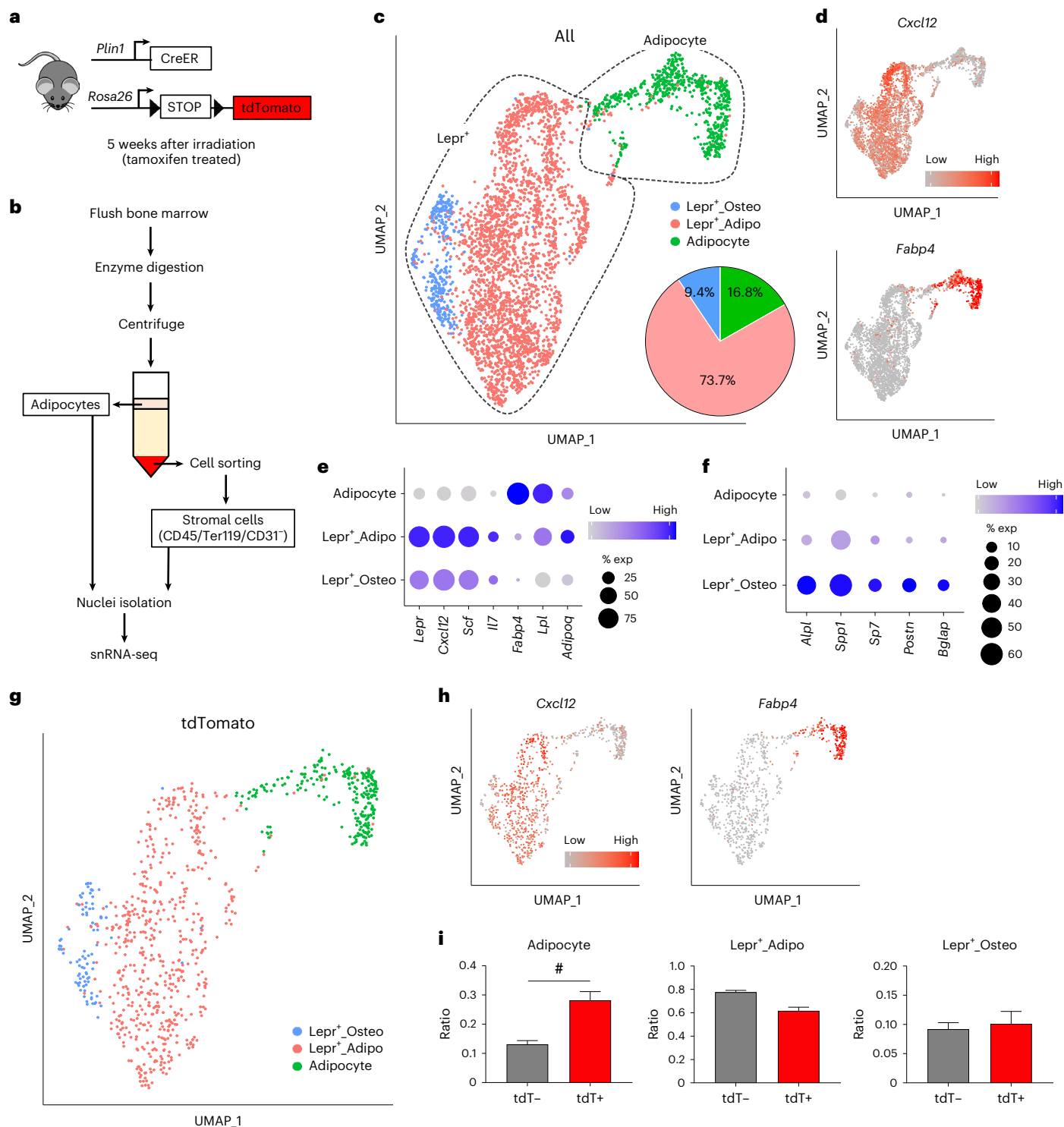
Fig. 3 | snRNA-seq reveals mesenchymal stromal cell populations in the regenerating bone marrow. a,b, Experimental scheme. Irradiated *Plin1^creER*; *Rosa26^LSL-tdTomato* mice were administrated tamoxifen on days 10, 12 and 14, and analyzed at 5 weeks postirradiation (**a**). Collected adipocytes and sorted CD45/ Ter119/CD31⁻ cells from the bone marrow of *Plin1^creER*; *Rosa26^LSL-tdTomato* mice were analyzed using snRNA-seq (**b**). **c**, Uniform manifold approximation and projection (UMAP) visualization of mesenchymal cells and their breakdown into two clusters (adipocyte, Lepr⁺). Lepr⁺ cells are further separated into Lepr⁺_Adipo and Lepr⁺_Osteo. The percentage of each cell cluster is shown. **d**, Gene expression levels of a mesenchymal stromal cell marker (*Cxcl12*) and an adipocyte marker (*Fabp4*) on UMAP. **e,f**, Dot plots showing the expression levels (% exp) of

mesenchymal stromal cell markers (*Lepr, Cxcl12, Scf* and *Il7*), adipocyte markers (*Fabp4* and *Lpl*), *Adipoq* (**e**) and osteolineage cell markers (*Alpl, Spp1, Sp7, Postn* and *Bglap*) (**f**). **g,h**, UMAP visualization of tdTomato⁺ cells (**g**) and expression levels of *Cxcl12* and *Fabp4* on UMAP (**h**). **i**, Proportion of tdTomato⁻ (tdT−) and tdTomato⁺ (tdT+) cells in adipocyte, Lepr⁺_Adipo and Lepr⁺_Osteo clusters, analyzed with scProportionTest package (*n* = 379 cells for tdT− adipocyte; *n* = 262 cells for tdT+ adipocyte; *n* = 2,245 cells for tdT− Lepr⁺_Adipo; *n* = 573 cells for tdT+ Lepr⁺_Adipo; *n* = 266 cells for tdT− Lepr⁺_Osteo; *n* = 94 cells for tdT+ Lepr⁺_Osteo). Cells were from two independent sequencing experiments on two independent mice each. Data are presented as mean ± 95% confidence interval. #, false discovery rate <0.05 and absolute log₂(fold change) >0.58.

failed to identify any tdTomato^{+} cells, suggesting that the labeling was specific to mature adipocytes (Extended Data Fig. 3d). However, when these mice were analyzed 6 weeks after tamoxifen administration, tdTomato[+] perilipin^{−} stromal cells were readily identified by whole-mount microscopy and flow cytometry (Extended Data Fig. 3e–h). The tdTomato[+] perilipin^{−} stromal cells were expressing LepR (Extended Data Fig. 3i). Thus, prominent bone marrow adipocyte dedifferentiation was also evident when a low dose of tamoxifen was used.

Similar to irradiation-mediated myeloablation, the number of bone marrow adipocytes also increased and then contracted following myeloablation mediated by 5-fluorouracil (5-FU) (Extended Data Fig. 4a,b). Bone marrow adipocytes also dedifferentiated to LepR^{+} stromal cells after 5-FU treatment (Extended Data Fig. 4c–f). These data suggest that dedifferentiation of bone marrow adipocytes to LepR^{+} cells is a common response to myeloablation induced by either irradiation or 5-FU treatment.

Single-nucleus RNA sequencing analysis of the fate of bone marrow adipocytes

scRNA-seq is a powerful tool to profile gene expression and understand cell fate changes. Although scRNA-seq analyses have been performed on bone marrow stroma[10–13], mature adipocytes were not captured, likely because of the incompatibility of their large size and fragility with the dissociation method[19]. We collected adipocytes and sorted CD45/Ter119/CD31^{−} cells from the bone marrow of tamoxifen-treated *Plin1*[creER/+]; *Rosa26*[LSL-tdTomato] mice 5 weeks after irradiation and performed single-nucleus RNA sequencing (snRNA-seq) (Fig. 3a,b). Total bone marrow mesenchymal cells were clustered into two distinct populations (Fig. 3c and Extended Data Fig. 5a). One represents mesenchymal stromal cells identified by high expression of *Lepr*, *Cxcl12* and *Kitl* (herein Lepr[+]); the other represents adipocytes identified by high expression of *Fabp4* and *Lpl* (Fig. 3c–e and Extended Data Fig. 5a,b). In line with the identity of mature adipocytes, cells within the adipocyte cluster also expressed high levels of *Plin1*, *Plin2* and *Plin4* (Extended Data Fig. 5c,d). Interestingly, adipocytes also expressed higher levels of lipolysis enzymes (*Atgl*, also known as patatin-like phospholipase domain-containing 2 or *Pnpla2*, *Lipe* and *Mgll*), adrenergic receptors (*Adrb2* and *Adrb3*) and *Il6ra*, compared with Lepr^{+} cells (Extended Data Fig. 5c–e). Within the Lepr[+] population, two clusters could be further identified. Lepr[+]_Adipo was defined by high expression of *Adipoq* and Lepr[+]_Osteo was defined by high expression of osteolineage markers, including *Alpl*, *Spp1* and *Sp7* (Fig. 3e,f).

The inclusion of tdTomato transcript allowed us to specifically assess the fate of bone marrow adipocytes during bone marrow regeneration in *Plin1*[creER/+]; *Rosa26*[LSL-tdTomato] mice. The identified tdTomato^{+} mesenchymal cells were also clustered into two distinct groups, mesenchymal stromal cells and adipocytes, similar to total mesenchymal cells (Fig. 3g,h). A significantly higher portion of tdTomato^{+} cells were adipocytes compared with tdTomato^{−} cells (Fig. 3i). Importantly, tdTomato[+] adipocyte-derived stromal cells distributed to Lepr[+]_Adipo and Lepr[+]_Osteo without bias compared with tdTomato^{−} cells (Fig. 3i). Thus, consistent with marker gene expression (Fig. 2f–l), snRNA-seq suggests that bone marrow adipocytes dedifferentiate to bone marrow LepR^{+} stromal cells during regeneration and adipocyte-derived mesenchymal stromal cells have similar lineage heterogeneity compared with other mesenchymal stromal cells.

Little potential of dedifferentiated stromal cells in vitro

We tested whether bone marrow adipocyte dedifferentiation could be directly captured. Time-lapse imaging on cultured bone marrow adipocytes from *Plin1*[creER/+]; *Rosa26*[LSL-tdTomato] mice at 15 days postirradiation demonstrated that tdTomato[+] adipocytes gradually lost lipid droplets, exhibited a stromal cell morphology and divided over time in vitro (Extended Data Fig. 6a,b).

Because LepR^{+} cells contain the vast majority of colony-forming unit-fibroblasts (CFU-Fs) and are heterogeneous[8], we wondered whether adipocyte-derived LepR^{+} cells have distinct functional properties. We initiated CFU-F and differentiation assays using enzymatically digested bone marrow cells from irradiated *Plin1*[creER/+]; *Rosa26*[LSL-tdTomato] mice at 8 weeks postirradiation (Extended Data Fig. 6c). Compared with tdTomato^{−} stromal cells, tdTomato[+] adipocyte-derived stromal cells had very limited capacity to proliferate and did not form CFU-F colonies with more than 25 cells (Extended Data Fig. 6d–f). Interestingly, despite limited proliferation, a significantly higher portion of tdTomato^{+} stromal cells spontaneously acquired lipid droplets compared with tdTomato^{−} stromal cells (Extended Data Fig. 6g,h), suggesting a skewed differentiation to adipocytes in vitro. Under osteodifferentiation culture conditions, no tdTomato^{+} stromal cells formed colony-forming unit-osteoblasts (CFU-Obs) colonies, although ~3% of attached tdTomato^{−} stromal cells did (Extended Data Fig. 6i,j). These data suggest that bone marrow adipocyte-derived stromal cells proliferate little and differentiate easily to adipocytes, but not osteolineage cells in vitro.

Adipocyte-derived cells become osteolineage cells in vivo

Although in vitro assays are useful at revealing cell potential, they may not capture the actual fate of tdTomato^{+} cells in vivo. To test whether mature adipocyte-derived cells could give rise to osteolineage cells in vivo, we irradiated and administered tamoxifen on days 10, 12 and 14 after irradiation to *Plin1*[creER/+]; *Rosa26*[LSL-tdTomato]; *Col2.3-GFP* mice where osteolineage cells are labeled with *Col2.3*-GFP[23] (Fig. 4a). At 10 weeks postirradiation, some *Col2.3*-GFP^{+} osteolineage cells were tdTomato[+] (Fig. 4b), suggesting that mature adipocyte-derived cells can give rise to osteolineage cells in vivo.

The modest contribution of adipocyte-derived cells to osteolineage cells might reflect the limited osteogenic activity of LepR^{+} cells in young adult mice[8]. Because bone injury promotes osteogenesis and an osteoblastic contribution by mesenchymal stromal cells[8,9,14], we adopted a drill-hole injury model[14,24]. We irradiated *Plin1*[creER/+]; *Rosa26*[LSL-tdTomato]; *Col2.3-GFP* mice to induce adipogenesis and labeled adipocytes through tamoxifen administration on days 10, 12 and 14 postirradiation. Eight weeks after irradiation, we injured the bone by drilling a small hole in the cortical region of the tibia (Fig. 4c). Two weeks later, the contribution of adipocyte-derived cells to osteolineage cells was assessed by whole-mount confocal imaging. Abundant tdTomato[+] mature

Fig. 4 | Adipocyte-derived mesenchymal stromal cells contribute to osteolineage cells. a, Experimental scheme. *Plin1*[creER]; *Rosa26*[LSL-tdTomato]; *Col2.3-GFP* mice were sublethally irradiated, treated with tamoxifen and analyzed at the indicated time. **b**, Representative images of trabecular bone (*n* = 3). Some *Col2.3*-GFP^{+} osteolineage cells were tdTomato[+] (arrows). **c**, Experimental scheme of a cortical bone injury induced by a drill-hole. **d**, Representative whole-mount confocal images of tibias. Dashed lines indicate cortical bone (CB). **e**, Enlarged images of the injury site from **d** and quantification of *Col2.3*-GFP^{+} osteolineage cells that were tdTomato^{+} cells at the injury site (*n* = 3). Some *Col2.3*-GFP^{+} osteolineage cells were tdTomato[+] (arrows). **f**, Experimental scheme of a trabecular bone injury induced by a drill-hole. **g**, Representative whole-mount confocal images of femurs. **h**, Enlarged images of the injury site from **g** and quantification of *Col2.3*-GFP^{+} cells that were tdTomato^{+} cells at the injury site (*n* = 3). Some *Col2.3*-GFP^{+} osteolineage cells were tdTomato+ (arrows). **i,j**, Representative flow cytometric plots showing that adipocyte-derived cells contributed to *Col2.3*-GFP^{+} osteolineage cells (*n* = 3) (**i**). RT–qPCR analyses showing the relative expression levels of osteolineage markers in sorted LepR^{+} (CD45/Ter119/CD31^{−}PDGFRα^{+}) bone marrow stromal cells (*n* = 4, LepR^{+}), tdTomato^{+}*Col2.3*-GFP^{+} osteolineage cells (*n* = 3, tdT (+) osb) and tdTomato^{−}*Col2.3*-GFP^{+} osteolineage cells (*n* = 3, tdT (−) osb) (**j**). All data represent mean ± s.d. mRNA, messenger RNA. Two-sided Student's *t*-tests were used in **j**. Scale bar, 50 μm (**b,e**), 100 μm (**h**), 200 μm (**d,g**), 5 mm (**c,f**). Squares indicate enlarged regions in **b, d, e, g** and **h**.

adipocyte-derived stromal cells were in the bone marrow independent of the injury and a prominent number of *Col2.3*-GFP⁺ osteolineage cells were at the injury site (Fig. 4d). Importantly, 15% of *Col2.3*-GFP⁺ osteolineage cells at the injury site were expressing tdTomato (Fig. 4d,e),

suggesting that adipocyte-derived cells substantially contribute to osteolineage cells following cortical bone injury. We also tested the contribution to osteolineage cells made by adipocyte-derived cells in the trabecular bone region. Similarly, about 15% of *Col2.3*-GFP⁺
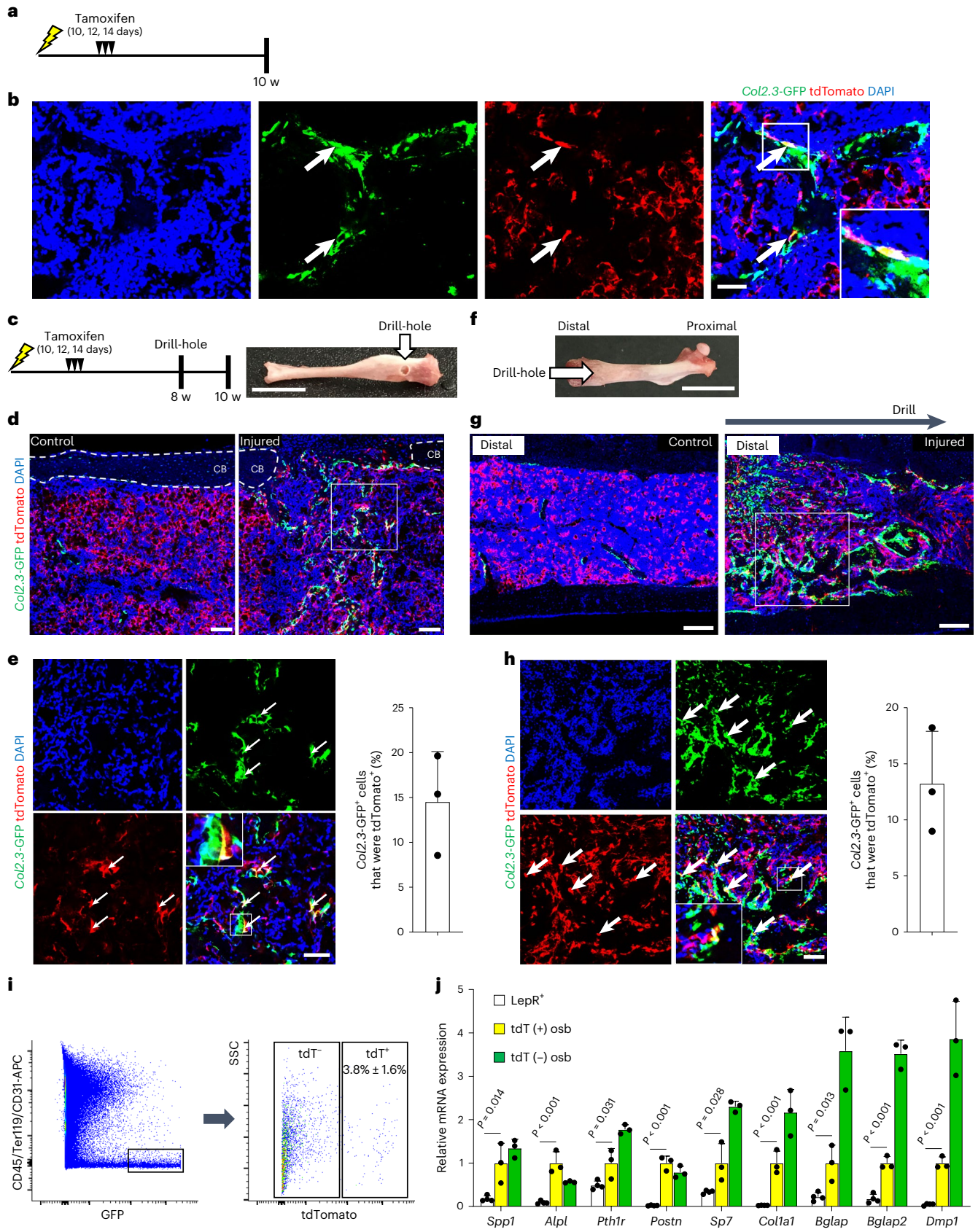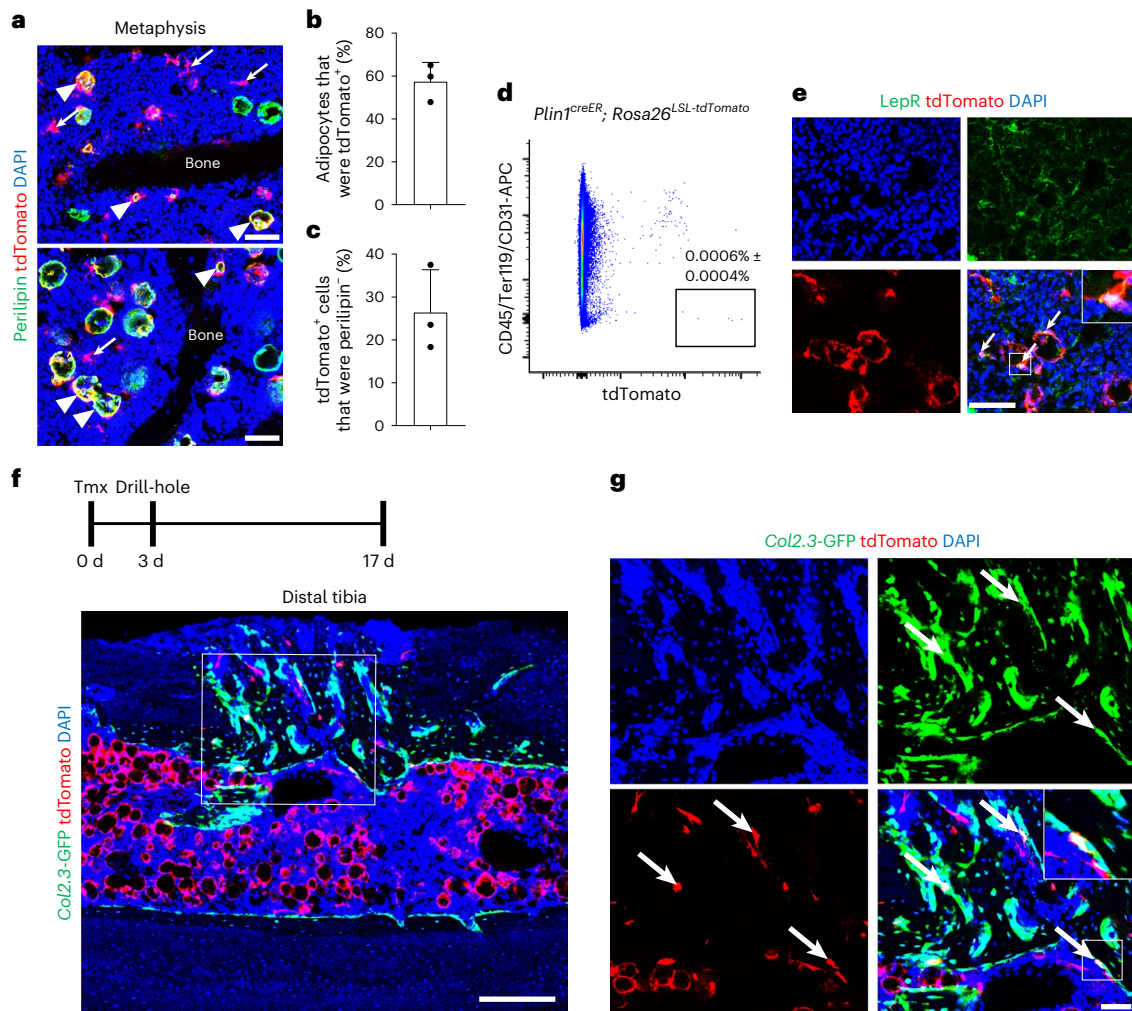
Fig. 5 | Bone marrow adipocytes can dedifferentiate to stromal cells and bone marrow adipocyte-derived cells can differentiate into osteolineage cells without myeloablation. **a**, *Plin1^{creER}; Rosa26$^{LSL-tdTomato}$* mice were analyzed 6 weeks after the administration of three doses of tamoxifen. Representative images of metaphasis showing that some tdTomato$^+$ cells were negative for perilipin (arrows). Triangles highlight some of the tdTomato$^+$ adipocytes. **b**, Frequency of perilipin$^+$ adipocytes that were tdTomato$^+$ from mice as in **a** ($n = 3$). **c**, Frequency of tdTomato$^+$ cells that were perilipin$^-$ from mice as in **a** ($n = 3$). **d**, Representative flow cytometric plot showing tdTomato$^+$ cells are present in enzymatically digested bone marrow cells of tibias from *Plin1^{creER}; Rosa26$^{LSL-tdTomato}$* mice 6 weeks after the administration of three doses of tamoxifen ($n = 3$). **e**, Representative confocal images showing that adipocyte-derived tdTomato$^+$ bone marrow stromal cells expressed LepR (arrows) 6 weeks after the administration of three doses of tamoxifen ($n = 3$). **f**, Representative image of drill-hole injured distal tibias from *Plin1^{creER}; Rosa26$^{LSL-tdTomato}$; Col2.3-GFP* mice ($n = 2$). Three days after tamoxifen (Tmx) administration, the adipocyte-rich distal tibia was injured by a drill-hole and analyzed 2 weeks later. **g**, Enlarged images of the injury site where some *Col2.3*-GFP$^+$ osteolineage cells were from tdTomato$^+$ adipocyte-derived cells without myeloablation (arrows). All data represent mean ± s.d. Scale bar, 50 µm (**a,e,g**), 200 µm (**f**). Squares indicate enlarged regions in **e–g**.

osteolineage cells at the injury site were derived from tdTomato$^+$ adipocytes (Fig. 4f–h). Compared with bone marrow LepR$^+$ cells, sorted tdTomato$^+$*Col2.3*-GFP$^+$ cells express significantly higher levels of osteolineage markers, including *Spp1, Alpl, Pth1r, Postn, Sp7, Col1a1, Bglap, Bglap2* and *Dmp1* (~2–47-fold), suggesting an osteolineage differentiation (Fig. 4i,j). However, tdTomato$^+$*Col2.3*-GFP$^+$ osteolineage cells appear to be less mature compared with tdTomato$^-$*Col2.3*-GFP$^+$ cells because they expressed lower levels of mature osteolineage cell markers such as *Bglap, Bglap2* and *Dmp1* (~3.5–3.9-fold) (Fig. 4j). This may reflect a high osteolineage differentiation barrier to be overcome by the adipocyte-derived stromal cells. Overall, our data suggest that bone marrow adipocytes have lineage plasticity and can give rise to osteolineage cells in vivo.

Bone marrow adipocytes are also plastic in the steady state

To test whether bone marrow adipocytes dedifferentiate independently of myeloablation in the steady state, we administrated three doses of tamoxifen to young adult *Plin1$^{creER/+}$; Rosa26$^{LSL-tdTomato}$* mice and

analyzed them 6 weeks later. A few adipocytes were concentrated in the metaphyseal region of the femur. Fewer than 60% of these adipocytes were tdTomato$^+$, suggesting that many new adipocytes are generated outside the tamoxifen induction window (Fig. 5a,b). In contrast to the specific labeling of adipocytes when analyzed at 36 h (Fig. 1k,l), 26% of tdTomato$^+$ cells were not perilipin$^+$ mature adipocytes but showed a stromal morphology when analyzed at 6 weeks after tamoxifen administration (Fig. 5a,c). Consistently, tdTomato$^+$ stromal cells could be detected by flow cytometry and they were expressing LepR (Fig. 5d,e). These data suggest that although new adipocytes are generated, mature adipocytes concurrently dedifferentiate to mesenchymal stromal cells independent of myeloablation in the steady state.

We also tested the contribution of adipocyte-derived cells to osteolineage cells without myeloablation. Because only a few adipocytes are in most of the bone marrow from young adult mice[25], the contribution of adipocyte-derived cells to osteolineage cells in these bones was likely minimal, if any. We focused on bone regions where adipocytes
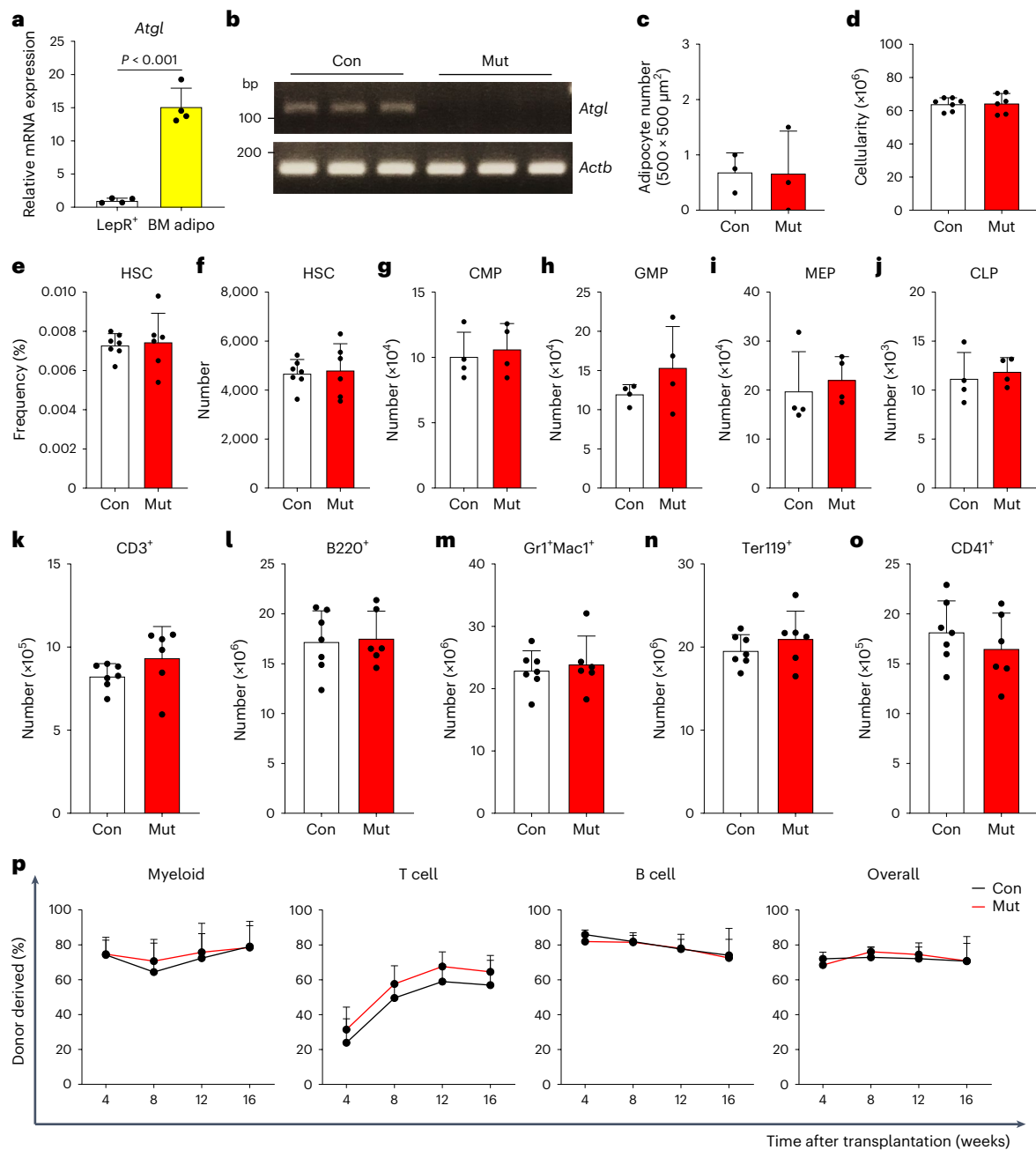
Fig. 6 | *Prx1-cre; Atgl^{fl/fl}* mice exhibit normal hematopoiesis in the steady state.
a, RT–qPCR analysis shows that *Atgl* is preferentially expressed by bone marrow adipocytes (BM adipo) compared with LepR⁺ stromal cells (LepR⁺) (*n* = 4 for each group). **b**, RT–PCR analysis shows that *Atgl* was efficiently deleted from bone marrow mesenchymal stromal cells of *Prx1-cre; Atgl^{fl/fl}* mice (*n* = 3). β-actin was used as a control. **c**, Number of adipocytes in the bone marrow (*n* = 3 for each group). **d–j**, Cellularity (**d**), HSC frequency (**e**), HSC number (**f**), CMP number (**g**), GMP number (**h**), MEP number (**i**) and CLP number (**j**) in the bone marrow (*n* = 7 for Con, *n* = 6 for Mut in **d–f**; *n* = 4 for each group in **g–j**). **k–o**, The number of CD3⁺ cells (**k**), B220⁺ cells (**l**), Gr1⁺Mac1⁺ cells (**m**), Ter119⁺ cells (**n**) and CD41⁺ cells (**o**) in the bone marrow (*n* = 7 for Con, *n* = 6 for Mut). **p**, Competitive transplantation of 5 × 10⁵ bone marrow cells from *Prx1-cre; Atgl^{fl/f}* or control mice along with 5 × 10⁵ competitor bone marrow cells. Donor chimeric levels of myeloid, T cells, B cells and overall cells in peripheral blood are shown (*n* = 9 recipient mice for Con, *n* = 10 recipient mice for Mut). Con, controls; Mut, *Prx1-cre; Atgl^{fl/fl}* mice. All data represent mean ± s.d. Two-sided Student's *t*-tests were used in **a** and **c–o**. Two-way ANOVA followed by Sidak's multiple comparison test was used in **p**.

are abundant in young adult mice. The distal end of the murine tibia contains a large number of adipocytes[26] and is easily accessible to bone injury. We performed a drill-hole injury to this region in young adult *Plin1^{creER/+}; Rosa26^{LSL-tdTomato}; Col2.3-GFP* mice. Two weeks after the injury, a notable number of *Col2.3*-GFP⁺ osteolineage cells at the injury site were tdTomato⁺, suggesting an adipocyte origin (Fig. 5f,g). Therefore, bone marrow adipocytes can give rise to osteolineage cells without myeloablation.

Adipocyte *Atgl* deletion depletes HSCs during regeneration
Because excessive lipid droplets are a hallmark of adipocytes and bone marrow adipocytes express high levels of lipolysis enzymes (Extended Data Fig. 5c,d), we reasoned that blocking lipolysis might obstruct bone marrow adipocyte dedifferentiation. *Atgl* encodes a key enzyme required for lipolysis[27] and was preferentially expressed by bone marrow adipocytes (Fig. 6a and Extended Data Fig. 5c,d). Because deletion of *Atgl* from adipocytes throughout the body leads to systemic
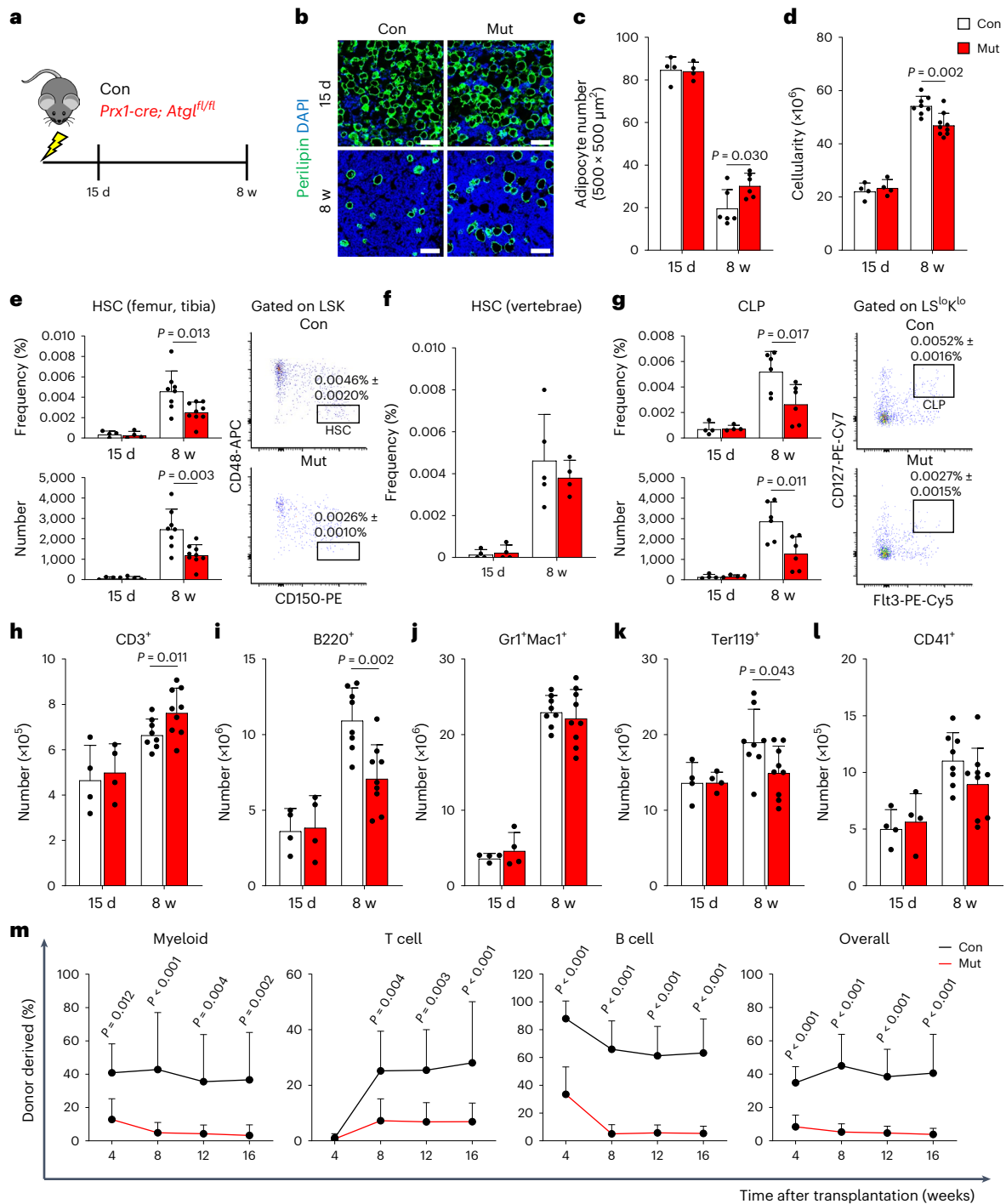
Fig. 7 | Conditional deletion of *Atgl* impedes adipocyte dedifferentiation and leads to HSC depletion from the bone marrow after irradiation.
a, Experimental scheme showing analysis of *Prx1-cre; Atgl^{fl/fl}* and control mice at 15 days (15 d) and 8 weeks (8 w) postirradiation. **b,c**, Representative images (**b**) and quantification (**c**) of bone marrow adipocytes in the diaphysis region. Adipocytes were stained with an anti-perilipin antibody (in green) (n = 4 for each group at 15 days, n = 6 for each group at 8 weeks postirradiation). Scale bar, 50 μm. **d**, Cellularity of femur and tibia at 15 days (n = 4 for each group) and 8 weeks (n = 8 for Con, n = 9 for Mut) postirradiation. **e**, HSC frequency and number in the femur and tibia at 15 days (n = 4 for each group) and 8 weeks (n = 8 for Con, n = 9 for Mut) postirradiation. Representative flow cytometric plots at 8 weeks postirradiation are shown. LSK, Lin⁻Sca1⁺cKit⁺. **f**, HSC frequency in the vertebrae at 15 days (n = 4 for each group) and 8 weeks (n = 5 for Con, n = 4

for Mut) postirradiation. **g**, CLP frequency and number in the femur and tibia at 15 days (n = 4 for each group) and 8 weeks (n = 6 for each group) postirradiation. Representative flow cytometric plots at 8 weeks postirradiation are shown. **h–l**, The number of CD3⁺ cells (**h**), B220⁺ cells (**i**), Gr1⁺Mac1⁺ cells (**j**), Ter119⁺ cells (**k**) and CD41⁺ cells (**l**) in the bone marrow at 15 days (n = 4 for each group) and 8 weeks (n = 8 for Con, n = 9 for Mut) postirradiation. **m**, Transplantation of bone marrow cells from *Prx1-cre; Atgl^{fl/f}* or control along with competitor bone marrow cells. Donor chimera levels of myeloid, T, B and overall cells are shown (n = 9 recipient mice for Con, n = 10 recipient mice for Mut). See detail in Extended Data Fig. 7p. Con, controls; Mut, *Prx1-cre; Atgl^{fl/fl}* mice. All data represent mean ± s.d. Two-sided Student's *t*-tests were used in **c–l**. Two-way ANOVA followed by Sidak's multiple comparison test was used in **m**.

metabolic phenotypes[28], we conditionally deleted *Atgl* from bone marrow mesenchymal stromal cells of the long bones by generating *Prx1-cre; Atgl*^{fl/fl} mice (Fig. 6b). Because *Prx1-cre* recombines in mesenchymal stromal cells of the long bones[2,6,29] and bone marrow adipocytes are derived from mesenchymal stromal cells[8], *Prx1-cre* also recombines in adipocytes of the long bones[30]. The *Prx1-cre; Atgl*^{fl/fl} mice thus allowed us to assess the role of *Atgl* in bone marrow mesenchymal lineage cells, including adipocytes, on HSCs and hematopoiesis. Steady-state young adult *Prx1-cre; Atgl*^{fl/fl} mice had normal bone marrow adipocyte number, cellularity, HSC frequency and number in the long bones compared with littermate controls (Fig. 6c–f). These mice also had comparable numbers of restricted progenitors, including CMPs, GMPs, MEPs and CLPs, as well as maturing hematopoietic cells in the bone marrow (Fig. 6g–o and Extended Data Fig. 7a–e). Bone marrow cells from the *Prx1-cre; Atgl*^{fl/fl} mice reconstituted recipient mice at levels comparable to controls (Fig. 6p). Thus, *Atgl* in the bone marrow stromal cells is not required for HSCs and hematopoiesis in young adult mice in the steady state.

We then irradiated young adult *Prx1-cre; Atgl*^{fl/fl} mice and littermate controls to induce myeloablation and subsequent hematopoietic regeneration. The mice were analyzed at 15 days postirradiation, when the number of adipocytes peaked, and 8 weeks postirradiation, when adipocyte dedifferentiation and HSC regeneration progressed to considerable levels (Figs. 1, 2 and 7a). Consistent with the role of *Atgl* in lipolysis but not lipogenesis, *Prx1-cre; Atgl*^{fl/fl} mice had similar levels of adipogenesis and hematopoiesis compared with controls at 15 days postirradiation (Fig. 7b–l and Extended Data Fig. 7f–i). However, conditional deletion of *Atgl* from bone marrow mesenchymal stromal lineage cells in *Prx1-cre; Atgl*^{fl/fl} mice led to more adipocytes and lower bone marrow cellularity in the long bones at 8 weeks postirradiation compared with littermate controls (Fig. 7b–d). As expected, these mice also had a reduction in bone marrow mesenchymal stromal cells (Extended Data Fig. 7j). HSC frequency and number in the long bones from *Prx1-cre; Atgl*^{fl/fl} mice were significantly lower compared with littermate controls at 8 weeks postirradiation (Fig. 7e). *Prx1-cre* also recombines in subcutaneous white adipocytes[31]. Thus, the observed HSC phenotypes could be due to a systemic effect from the deletion of *Atgl* in subcutaneous white adipocytes. However, *Prx1-cre* does not recombine in vertebral bones[29] and HSC frequency in vertebral bones did not differ between *Prx1-cre; Atgl*^{fl/fl} mice and controls (Fig. 7f), ruling out a systemic effect. Although the numbers of CMP, GMP and MEP were comparable (Extended Data Fig. 7f–i), CLP number was significantly reduced in *Prx1-cre; Atgl*^{fl/fl} mice compared with controls at 8 weeks postirradiation (Fig. 7g). *Prx1-cre; Atgl*^{fl/fl} mice also had significant reduction in B220^{+} B cell frequency and number, and modest increases in CD3^{+} T cell frequency and number in the bone marrow (Fig. 7h,i and Extended Data Fig. 7k,l). The frequency and number of Gr1^{+}Mac1^{+} myeloid and CD41^{+} megakaryocytic cells were largely normal, whereas the number of Ter119^{+} erythroid cells was modestly reduced (Fig. 7j–l and Extended Data Fig. 7m–o). We transplanted bone marrow cells from regenerating *Prx1-cre; Atgl*^{fl/fl} and littermate control mice at 8 weeks postirradiation together with competitor cells into lethally irradiated recipient mice (Extended Data Fig. 7p). Bone marrow cells from irradiated *Prx1-cre; Atgl*^{fl/fl} mice gave significantly lower multilineage reconstitution compared with controls (Fig. 7m). Taken together, these data suggest that adipocyte dedifferentiation promotes HSC regeneration and lymphoid differentiation after myeloablation in the bone marrow.

Discussion

Adiponectin has been widely used as a marker for mature adipocytes. However, bone marrow LepR^{+} cells also express adiponectin at high levels (Extended Data Fig. 2a–e and refs. 10–13), rendering it unsuitable as a marker to specifically label adipocytes in the bone marrow. By contrast, perilipin is specifically expressed by mature adipocytes but not any other cells in the bone marrow (Fig. 1k,l and Extended Data Fig. 2). Because perilipin is required for adipocyte development[32],

we used a *P2A-creER* knock-in strategy to drive the expression of *creER* specifically in adipocytes without disrupting the expression of perilipin (Extended Data Fig. 2f–h). Our *Plin1*[creER] mice allow specific tracing of the fate of bone marrow adipocytes.

In vitro CFU-F assays suggest that tdTomato[+] adipocyte-derived stromal cells have limited colony formation capacity with no osteodifferentiation (forming CFU-Obs), at least under our assay condition (Extended Data Fig. 6). However, our in vivo lineage tracing analyses demonstrate that tdTomato[+] adipocytes dedifferentiate to LepR^{+} cells and these tdTomato^{+} cells can become osteolineage cells (Figs. 2–4), highlighting the advantage of these assays in assessing cell fate.

The role of bone marrow adipocytes in hematopoiesis was unclear. Although the level of adipogenesis is negatively correlated with hematopoiesis in the steady state[25], adipocytes promote HSC and hematopoietic recovery shortly after irradiation (4 weeks) when bone marrow mesenchymal stromal cells are depleted[17]. Bone marrow adipocytes express *Scf* and *Cxcl12* (Figs. 2j and 3e), albeit at significantly lower levels compared with LepR^{+} cells, suggesting that adipocytes are less capable at maintaining HSCs relative to LepR^{+} cells. We envision that adipogenesis is a stress response and promotes hematopoietic recovery shortly after myeloablation. As hematopoiesis gradually restores, suboptimal HSC-supporting adipocytes need to be replaced by LepR^{+} cells. The cellular plasticity of the bone marrow niche may accommodate distinct functional requirements by hematopoiesis and HSCs in the steady state and during stress.

It is not clear what molecular mechanisms regulate adipocyte plasticity. Upon irradiation, *Prx1-cre; Atgl*^{fl/fl} mice exhibited accumulated adipocytes, defective lymphopoiesis and declined HSC function (Fig. 7), all features of the aging bone marrow[33–36]. Interestingly, marrow adipocytes preferentially express receptors for adrenergic and IL-6 signaling (Extended Data Fig. 5c–e), which have been implicated in inflammation and/or lipolysis in adipocytes[37,38]. These data suggest that inflammation may be a driving factor. Likewise, inflammation (for example, IL-17) propels osteogenesis after bone injury[39]. Epigenetic mechanisms may be involved as well.

We demonstrate that adipocyte-derived cells can become osteolineage cells (Fig. 4). Given that bone marrow adipocytes dedifferentiate to LepR^{+} cells (Fig. 2), progenitors of osteolineage cells in adults[8], adipocyte-derived cells likely first dedifferentiate to mesenchymal stromal cells and then differentiate to osteolineage cells. Further studies are needed to test whether direct transdifferentiation occurs. Although substantial adipocyte dedifferentiation also occurs in the steady state (Fig. 5), the role of bone marrow adipocytes in young homeostatic mice is likely limited, because only a few adipocytes are present in most of the bone marrow. However, humans have abundant bone marrow adipocytes, even at a young age[17,40], suggesting a potentially much greater contribution of bone marrow adipocytes to skeletal and hematopoietic homeostasis. The cellular plasticity of bone marrow adipocytes (dedifferentiation and transdifferentiation) offers enormous potential for regenerative medicine.

Online content

Any methods, additional references, Nature Portfolio reporting summaries, source data, extended data, supplementary information, acknowledgements, peer review information; details of author contributions and competing interests; and statements of data and code availability are available at https://doi.org/10.1038/s41588-023-01528-2.

References

1. Ding, L., Saunders, T. L., Enikolopov, G. & Morrison, S. J. Endothelial and perivascular cells maintain haematopoietic stem cells. *Nature* **481**, 457–462 (2012).
2. Ding, L. & Morrison, S. J. Haematopoietic stem cells and early lymphoid progenitors occupy distinct bone marrow niches. *Nature* **495**, 231–235 (2013).

3. Lee, Y., Decker, M., Lee, H. & Ding, L. Extrinsic regulation of hematopoietic stem cells in development, homeostasis and diseases. *Wiley Interdiscip. Rev. Dev. Biol.* **6**, https://doi.org/10.1002/wdev.279 (2017).

4. Comazzetto, S., Shen, B. & Morrison, S. J. Niches that regulate stem cells and hematopoiesis in adult bone marrow. *Dev. Cell* **56**, 1848–1860 (2021).

5. Sugiyama, T., Kohara, H., Noda, M. & Nagasawa, T. Maintenance of the hematopoietic stem cell pool by CXCL12–CXCR4 chemokine signaling in bone marrow stromal cell niches. *Immunity* **25**, 977–988 (2006).

6. Greenbaum, A. et al. CXCL12 in early mesenchymal progenitors is required for haematopoietic stem-cell maintenance. *Nature* **495**, 227–230 (2013).

7. Cordeiro Gomes, A. et al. Hematopoietic stem cell niches produce lineage-instructive signals to control multipotent progenitor differentiation. *Immunity* **45**, 1219–1231 (2016).

8. Zhou, B. O., Yue, R., Murphy, M. M., Peyer, J. G. & Morrison, S. J. Leptin-receptor-expressing mesenchymal stromal cells represent the main source of bone formed by adult bone marrow. *Cell Stem Cell* **15**, 154–168 (2014).

9. Shu, H. S. et al. Tracing the skeletal progenitor transition during postnatal bone formation. *Cell Stem Cell* **28**, 2122–2136.e3 (2021).

10. Baryawno, N. et al. A cellular taxonomy of the bone marrow stroma in homeostasis and leukemia. *Cell* **177**, 1915–1932.e16 (2019).

11. Baccin, C. et al. Combined single-cell and spatial transcriptomics reveal the molecular, cellular and spatial bone marrow niche organization. *Nat. Cell Biol.* **22**, 38–48 (2020).

12. Tikhonova, A. N. et al. The bone marrow microenvironment at single-cell resolution. *Nature* **569**, 222–228 (2019).

13. Zhong, L. et al. Single cell transcriptomics identifies a unique adipose lineage cell population that regulates bone marrow environment. *eLife* **9**, e54695 (2020).

14. Matsushita, Y. et al. A Wnt-mediated transformation of the bone marrow stromal cell identity orchestrates skeletal regeneration. *Nat. Commun.* **11**, 332 (2020).

15. Chen, Q. et al. Apelin(+) endothelial niche cells control hematopoiesis and mediate vascular regeneration after myeloablative injury. *Cell Stem Cell* **25**, 768–783.e6 (2019).

16. Hooper, A. T. et al. Engraftment and reconstitution of hematopoiesis is dependent on VEGFR2-mediated regeneration of sinusoidal endothelial cells. *Cell Stem Cell* **4**, 263–274 (2009).

17. Zhou, B. O. et al. Bone marrow adipocytes promote the regeneration of stem cells and haematopoiesis by secreting SCF. *Nat. Cell Biol.* **19**, 891–903 (2017).

18. Bowers, E. et al. Granulocyte-derived TNFalpha promotes vascular and hematopoietic regeneration in the bone marrow. *Nat. Med.* **24**, 95–102 (2018).

19. Emont, M. P. et al. A single-cell atlas of human and mouse white adipose tissue. *Nature* **603**, 926–933 (2022).

20. Hagberg, C. E. et al. Flow cytometry of mouse and human adipocytes for the analysis of browning and cellular heterogeneity. *Cell Rep.* **24**, 2746–2756.e5 (2018).

21. Ye, R. et al. Impact of tamoxifen on adipocyte lineage tracing: inducer of adipogenesis and prolonged nuclear translocation of Cre recombinase. *Mol. Metab.* **4**, 771–778 (2015).

22. Jeffery, E. et al. The adipose tissue microenvironment regulates depot-specific adipogenesis in obesity. *Cell Metab.* **24**, 142–150 (2016).

23. Kalajzic, Z. et al. Directing the expression of a green fluorescent protein transgene in differentiated osteoblasts: comparison between rat type I collagen and rat osteocalcin promoters. *Bone* **31**, 654–660 (2002).

24. Matsushita, Y. et al. CCN3 protein participates in bone regeneration as an inhibitory factor. *J. Biol. Chem.* **288**, 19973–19985 (2013).

25. Naveiras, O. et al. Bone-marrow adipocytes as negative regulators of the haematopoietic microenvironment. *Nature* **460**, 259–263 (2009).

26. Scheller, E. L. et al. Region-specific variation in the properties of skeletal adipocytes reveals regulated and constitutive marrow adipose tissues. *Nat. Commun.* **6**, 7808 (2015).

27. Haemmerle, G. et al. Defective lipolysis and altered energy metabolism in mice lacking adipose triglyceride lipase. *Science* **312**, 734–737 (2006).

28. Ahmadian, M. et al. Desnutrin/ATGL is regulated by AMPK and is required for a brown adipose phenotype. *Cell Metab.* **13**, 739–748 (2011).

29. Logan, M. et al. Expression of Cre recombinase in the developing mouse limb bud driven by a Prxl enhancer. *Genesis* **33**, 77–80 (2002).

30. Horowitz, M. C. et al. Bone marrow adipocytes. *Adipocyte* **6**, 193–204 (2017).

31. Sanchez-Gurmaches, J., Hsiao, W. Y. & Guertin, D. A. Highly selective in vivo labeling of subcutaneous white adipocyte precursors with Prx1-Cre. *Stem Cell Rep.* **4**, 541–550 (2015).

32. Martinez-Botas, J. et al. Absence of perilipin results in leanness and reverses obesity in Lepr(db/db) mice. *Nat. Genet.* **26**, 474–479 (2000).

33. Snoeck, H. W. Aging of the hematopoietic system. *Curr. Opin. Hematol.* **20**, 355–361 (2013).

34. Rossi, D. J. et al. Cell intrinsic alterations underlie hematopoietic stem cell aging. *Proc. Natl Acad. Sci. USA* **102**, 9194–9199 (2005).

35. Verovskaya, E. V., Dellorusso, P. V. & Passegue, E. Losing sense of self and surroundings: hematopoietic stem cell aging and leukemic transformation. *Trends Mol. Med.* **25**, 494–515 (2019).

36. Ambrosi, T. H. et al. Adipocyte Accumulation in the Bone Marrow during Obesity and Aging Impairs Stem Cell-Based Hematopoietic and Bone Regeneration. *Cell Stem Cell* **20**, 771–784.e6 (2017).

37. Grabner, G. F., Xie, H., Schweiger, M. & Zechner, R. Lipolysis: cellular mechanisms for lipid mobilization from fat stores. *Nat. Metab.* **3**, 1445–1465 (2021).

38. Perry, R. J. et al. Hepatic acetyl CoA links adipose tissue inflammation to hepatic insulin resistance and type 2 diabetes. *Cell* **160**, 745–758 (2015).

39. Ono, T. et al. IL-17-producing gammadelta T cells enhance bone regeneration. *Nat. Commun.* **7**, 10928 (2016).

40. Justesen, J. et al. Adipocyte tissue volume in bone marrow is increased with aging and in patients with osteoporosis. *Biogerontology* **2**, 165–171 (2001).

Methods

Mice

Prx1-cre[29], *Rosa26*[LSL-tdTomato] (ref. [41]), *Col2.3-GFP*[23], *Pdgfrα*[GFP] (ref. [42]) and *Atgl*[fl] (ref. [43]) mice were obtained from the Jackson Laboratory and maintained on C57BL/6 background. *Plin1*[creER] mice were generated by gene targeting in B6 embryonic stem cells (FL19) and kept on a C57BL/6 background. The Cre activity in *Plin1*[creER] mice was induced by oral gavaging with tamoxifen (APExBIO) in corn oil (Sigma) for one or three doses. Two milligrams of tamoxifen was administered unless otherwise noted. Both male and female mice were included for analysis and no differences were appreciated. Young adult mice (8–10 weeks old) were used for experiments unless noted otherwise. All mice were housed in a specific pathogen-free, Association for the Assessment and Accreditation of Laboratory Animal Care-approved unit at Columbia University Medical Center with water and food (Purina Mouse Diet 5053) ad libitum. The facility is maintained at 20–22 °C and 30–60% humidity with a 12 h dark–light cycle. All protocols were approved by the Columbia University Institutional Animal Care and Use Committee.

Genotyping PCR primers

The primers used for genotyping *Plin1*[creER] are included in Supplementary Table 1.

Irradiation and 5-FU treatment

Young adult mice (8–10 weeks old) were sublethally irradiated (6 Gy) using a MultiRad 225 X-ray irradiator (Precision X-Ray). For 5-FU treatment, young adult mice were intraperitoneally injected with 150 mg per kg (body weight) 5-FU (Fresenius Kabi).

Bone marrow adipocyte isolation

Bone marrow adipocytes were isolated according to Fan et al.[44]. Dissected long bones from irradiated mice at 8–10 weeks old or nonirradiated wild-type mice at 6 months old (because the number of bone marrow adipocytes in young adult nonirradiated mice was very small, 6-month-old wild-type mice were used to isolate adipocytes) were washed in PBS buffer and cut at the ends. Bone marrow was flashed by centrifuge (5,000*g*, 1 s, room temperature), followed by digesting with Collagenase I (1 mg ml⁻¹; Worthington Biochemical), Collagenase IV (200 U ml⁻¹; Worthington Biochemical) and DNase I (200 U ml⁻¹; Sigma) at 37 °C for 20 min. Digested bone marrow was centrifuged and supernatant including adipocytes was put in PBS to wash. Floating adipocytes were then carefully collected for culture or RNA extraction.

snRNA-seq

Bone marrow adipocytes and sorted cells including bone marrow stromal cells (CD45/Ter119/CD31⁻) were kept frozen until nuclei isolation. Frozen cell pellets were resuspended in 1 ml of TST buffer (10 mM Tris–HCl (pH 7.4), 150 mM NaCl, 1 mM CaCl₂, 21 mM MgCl₂, 0.03% Tween-20, 0.01% BSA) and incubated for 10 min on ice. After adding 4 ml of ST buffer (10 mM Tris–HCl (pH 7.4), 150 mM NaCl, 1 mM CaCl₂, 21 mM MgCl₂), the solution was filtered through a 40-µm nylon mesh and then centrifuged (500*g*, 5 min) to obtain nuclei. Isolated nuclei were loaded into the 10x Chromium system and libraries were constructed using Chromium Single Cell 3′ Reagent Kit (v.3) according to the manufacturer's protocol. Libraries were subsequently sequenced on a NovaSeq 6000 Sequencing System (Illumina). The sequencing data were demultiplexed and converted to FASTQ format using the Cell Ranger pipeline (10x Genomics). Transcripts were aligned to a custom mm10/GRCm38 genome including the sequence of tdTomato-WPRE. Intronic reads are mapped as well as exonic reads and ambient RNA was removed with CellBender (v.0.2.2)[45]. Using the Seurat (v.4.2.0) package, low-quality cells were filtered out by nUMI >= 500, nGene >= 400, log10GenesPerUMI > 0.9, mitoRatio < 0.15 and RiboRatio < 0.05

filtering conditions. The doublets were then removed with Double-Finder (v.2.0.3)[46]. The above quality control steps were performed on individual samples. SCTransform was used to normalize data, scale data and find the top 3,000 feature genes, regressing out cell cycle, mitochondrial and ribosomal genes. IntegrateData was applied to integrate data from independent experiments. RunPCA and runUMAP were used for dimension reduction. FindClusters was then applied for cell clustering. Markers for each cluster were identified with FindConservedMarkers. We focused on LepR⁺ cells and adipocytes by removing other cell clusters. The remaining cells were analyzed with Seurat again as mentioned above. Cells with a tdTomato count above 0 were called tdTomato⁺ cells. The AddModuleScore function was used to calculate module scores. A heatmap was generated with the Scillus package (v.0.5.0) (https://scillus.netlify.app/). Statistical analyses of proportions in each cluster between tdTomato⁻ and tdTomato⁺ cells were performed with the scProportionTest package (v.0.0.0.9000) (https://github.com/rpolicastro/scProportionTest).

Bone marrow adipocyte culture

Freshly isolated bone marrow adipocytes were cultured in 25-ml flasks filled with MEM-α (Gibco) with 1% penicillin/streptomycin (Gibco), 20% heat-inactivated FBS (GeminiBio) and 10 µM ROCK inhibitor (Selleck), changing the media every 2–3 days. Cell cultures were maintained at 37 °C with 5% O₂ and 5% CO₂. The flask was turned upside down at the time when floating adipocytes attached to the top of the flask (day 2). The live adipocytes were then tracked by confocal microscopy (Leica Application Suite X, v.3.5.7.23225) from day 2 to day 7. LipiDye II (Funakoshi) was used according to the manufacturer's protocol to detect lipid droplets in live adipocytes.

CFU-F assay

Digested bone marrow cells from sublethally irradiated mice (8 weeks after irradiation) were plated at a clonal density in six-well plates or 25-ml flasks. Cells were cultured in MEM-α with 1% penicillin/streptomycin, 20% heat-inactivated FBS and 10 µM ROCK inhibitor, changing the media every 2–3 days. Cell cultures were maintained at 37 °C with 5% O₂ and 5% CO₂. On day 1, the culture media were changed and attached stromal cells were counted based on morphology. On day 12, colonies were stained using crystal violet (Thermo Scientific Chemicals). Colonies containing more than 25 cells were counted.

CFU-Ob assay

Digested bone marrow cells from sublethally irradiated mice (8 weeks after irradiation) were plated at a clonal density in six-well plates or 25-ml flasks. Cells were cultured in MEM-α with 1% penicillin/streptomycin and 10% heat-inactivated FBS. Cell cultures were maintained at 37 °C with 5% CO₂. On day 1, the culture media were changed and attached stromal cells were counted based on morphology. On day 12, the culture media were replaced with osteolineage differentiation media with 50 µg ml⁻¹ ascorbic acid (Sigma) and 10 mM β-glycerophosphate (Sigma). The media were changed every 2–3 days. At day 26, colonies were stained with Alizarin Red S (Sigma).

Drill-hole injury

Drill-hole injury was performed according to Matsushita et al.[14]. Briefly, mice were anesthetized by 2% isoflurane (Covetrus) with oxygen. The proximal or distal part of a tibia was drilled for cortical injury. The skin covering the tibia was incised and muscles attached to the site where the drill-hole would be made were stripped away. The tibia was then drilled with a 0.6-mm diameter drill. The incisions were closed using wound clips. The distal part of a femur was drilled for trabecular injury. Skin and part of cruciate ligaments were incised and the femur was drilled with a 0.6-mm diameter drill along the long axis. The incisions were closed by wound clips. Mice were analyzed at 2 weeks postinjury.

Osteolineage cell isolation

Bones containing injured regions were cut and followed by digesting with Liberase (0.65 units ml^{-1}; Sigma) in Ca^{2+}- and Mg^{2+}-free Hanks' balanced salt solution at 37 °C for 20 min in a shaking incubator (250 r.p.m., MAXQ 6000; Thermo Fisher Scientific). Cells were filtered through a 70-μm nylon mesh. These steps were repeated twice. Collected cells were stained with following antibodies: anti-CD45 (1:400, 30-F11; BioLegend), anti-Ter119 (1:200, TER-119; BioLegend) and anti-CD31 (1:200, 390; BioLegend).

Flow cytometry

For analyzing hematopoietic cells, bone marrow cells were isolated by flushing long bones (femur and tibia). The cells were passed through 25G syringes with Ca^{2+}- and Mg^{2+}-free Hanks' balanced salt solution with 2% heat-inactivated bovine serum for a single-cell suspension. Cells were filtered through a 70-μm nylon mesh. For staining HSCs, the following antibodies were used: lineage markers (anti-Ter119 (1:200, TER-119), anti-B220 (1:400, 6B2), anti-Gr1 (1:400, 8C5), anti-CD2 (1:200, RM2-5), anti-CD3 (1:200, 17A2), anti-CD5 (1:400, 53-7.3) and anti-CD8 (1:400, 53-6.7)), and anti-CD150 (1:200, TC15-12F12.2), anti-CD48 (1:200, HM48-1), anti-Sca-1 (1:200, E13-161.7) and anti-cKit (1:200, 2B8) (all from BioLegend). For staining hematopoietic progenitors, the following antibodies were used: lineage markers (anti-Ter119 (1:200, TER-119), anti-B220 (1:400, 6B2), anti-Gr1 (1:400, 8C5), anti-CD2 (1:200, RM2-5), anti-CD3 (1:200, 17A2), anti-CD5 (1:400, 53-7.3) and anti-CD8 (1:400, 53-6.7)), anti-Sca-1 (1:200, D7), anti-cKit (1:200, 2B8), Flt3 (1:100, A2F10), CD16/32 (1:200, 93), CD127 (1:200, A7R34) (all from BioLegend) and anti-CD34 (1:100, RAM34, from BD Biosciences). For staining mature cells, the following antibodies were used: anti-CD3 (1:200, 17A2), anti-B220 (1:400, 6B2), anti-Gr1 (1:400, 8C5), anti-Mac1 (1:400, M1/70), anti-Ter119 (1:200, TER-119) and anti-CD41 (1:200, MWReg30) (all from BioLegend). For analyzing and sorting stromal cells, bone marrow was flashed by centrifuge (5,000g, 1 s, room temperature) and followed by digesting with Collagenase I (1 mg ml^{-1}), Collagenase IV (200 U ml^{-1}) and DNase I (200 U ml^{-1}) at 37 °C for 20 min. Cells were then filtered through a 70-μm nylon mesh. Anti-CD140a (1:100, APA5), anti-CD45 (1:400, 30-F11), anti-Ter119 (1:200, TER-119) and anti-CD31 (1:200, 390) (all from BioLegend) antibodies were used to stain stromal cells. DAPI was used to preclude dead cells. Samples were run on FACSAria II, BD LSR II or FACSCelesta flow cytometers. FACSDiva (BD, v.9) or FlowJo (Tree Star, v.10.8.1) software was used for data analysis.

Intercellular staining

Digested bone marrow cells were fixed and permeabilized with BD Cytofix/Cytoperm buffer (BD Biosciences). Cells were then incubated with anti-CXCL12 antibody (1:100, 79018; R&D) or immunoglobulin G1 isotype control (MOPC-21; BioLegend).

Whole-mount immunostaining

Whole-mount immunostaining was performed as previously described[47]. Briefly, dissected long bones were washed in PBS and fixed overnight in 4% paraformaldehyde at 4 °C. Fixed bones were embedded in Optimal Cutting Temperature compound (Tissue-Tek) and snap frozen. Bones were sectioned by a cryostat and left at room temperature until the Optimal Cutting Temperature compound was fully melted. Specimens were fixed in 4% paraformaldehyde at 4 °C for 15 min and then blocked in PBS with 5% goat or donkey serum at room temperature for 30 min. Specimens were stained with primary antibodies for 1–2 days, followed by staining with secondary antibodies at room temperature for 2 h. The nuclei were stained with DAPI. Rabbit anti-perilipin-1 (1:300, D1D8; Cell Signaling), goat anti-LepR (1:100; R&D), goat anti-IL-7 (1:100; R&D) and rabbit anti-cleaved caspase-3 (Alexa Fluor 488 conjugated) (1:100; Cell Signaling) were used as primary antibodies. Unless otherwise mentioned, bone marrow of the diaphysis region, where the adipocyte number is low in the steady state but increases drastically upon irradiation, was analyzed.

RT–PCR and RT–qPCR

Cells were sorted directly into TRIzol (Ambion). Tissues were homogenized in TRIzol. Total RNA was purified according to the manufacturer's instructions and subjected to reverse transcription using SuperScript III Reverse Transcriptase (Invitrogen) or GoScript Reverse Transcriptase (Promega). The resulting complementary DNAs were used for PCR or qPCR. Gene expression was assessed by PCR using GoTaq qPCR Master Mix (Promega) on a CFX Connect Real-Time PCR Detection System (Bio-Rad) and analyzed with CFX Manager (v.3.1) and Excel (Microsoft, 2019). β-actin was used to normalize the expression of genes. Primers used in this study are included in Supplementary Table 1.

TUNEL staining

Apoptotic adipocytes in the bone marrow were labeled by TUNEL staining. One-step TUNEL Apoptosis Kit (Elabscience) was used according to the manufacturer's protocol.

Bone marrow transplantation assay

Adult recipient mice were lethally irradiated using a MultiRad 225 X-ray irradiator (Precision) with a total of 1,050 rads in a split dose delivered 2 h apart. Cells were transplanted by retro-orbital venous sinus injection of anesthetized mice. Donor bone marrow cells were transplanted along with recipient bone marrow cells into lethally irradiated recipient mice. Recipient bone marrow cells were from mice that were treated similarly to the donor mice. Mice were maintained on antibiotic water (Baytril 0.17 g l^{-1}, Bayer) for 14 days then switched to regular water. Recipient mice were bled to assess the level of donor-derived blood lineages, including myeloid, B and T cells. Blood cells were subjected to ammonium chloride potassium red cell lysis before antibody staining. Antibodies including anti-CD45.2 (1:400, 104), anti-CD45.1 (1:200, A20), anti-CD3 (1:200, 17A2), anti-B220 (1:400, 6B2) and anti-Gr1 (1:400, 8C5) (all from BioLegend) were used to stain cells.

Statistics and reproducibility

Statistical methods were as described in figure legends. GraphPad Prism (v.6.3.1) or Excel (2019) was used for statistical analyses unless noted otherwise. No statistical method was used to predetermine sample sizes, which were based on previous research experiences for similar assays[48–51]. Data distribution was assumed to be normal but this was not formally tested. Throughout the text, n stands for independent animals in independent experiments, except in Fig. 3, where n stands for the number of single cells analyzed. No data were excluded from the analysis. All experiments with quantification data were repeated with at least three independent biological replicates in independent experiments. All replications were successful, with similar results. Mice with desired genotypes/treatments were randomly chosen for analysis. The investigators were not blinded to allocation during experiments and outcome assessment.

Ethics declarations

All experimental protocols were approved by the Columbia University Institutional Animal Care and Use Committee. All experiments were performed in accordance with guidelines and regulations.

Reporting summary

Further information on research design is available in the Nature Portfolio Reporting Summary linked to this article.

Data availability

The snRNA-seq data generated by this study have been deposited in the NCBI Gene Expression Omnibus (GEO) repository under accession number GSE227255. Source data are provided with this paper.

Code availability

Standard bioinformatics pipelines used for analyzing snRNA-seq data were described in the 'snRNA-seq' section. All codes that have been used in the study are available at https://doi.org/10.5281/zenodo.8280830 (ref. 52) and https://github.com/LeiDingLab/Nature_Genetics_2023.

References

41. Madisen, L. et al. A robust and high-throughput Cre reporting and characterization system for the whole mouse brain. *Nat. Neurosci.* **13**, 133–140 (2010).

42. Hamilton, T. G., Klinghoffer, R. A., Corrin, P. D. & Soriano, P. Evolutionary divergence of platelet-derived growth factor alpha receptor signaling mechanisms. *Mol. Cell. Biol.* **23**, 4013–4025 (2003).

43. Haemmerle, G. et al. ATGL-mediated fat catabolism regulates cardiac mitochondrial function via PPAR-alpha and PGC-1. *Nat. Med.* **17**, 1076–1085 (2011).

44. Fan, Y. et al. Parathyroid hormone directs bone marrow mesenchymal cell fate. *Cell Metab.* **25**, 661–672 (2017).

45. Fleming, S. J. et al. Unsupervised removal of systematic background noise from droplet-based single-cell experiments using CellBender. *Nat. Methods* **20**, 1323–1335 (2023).

46. McGinnis, C. S., Murrow, L. M. & Gartner, Z. J. DoubletFinder: doublet detection in single-cell RNA sequencing data using artificial nearest neighbors. *Cell Syst.* **8**, 329–337.e4 (2019).

47. Sacma, M. et al. Haematopoietic stem cells in perisinusoidal niches are protected from ageing. *Nat. Cell Biol.* **21**, 1309–1320 (2019).

48. Gao, L., Decker, M., Chen, H. & Ding, L. Thrombopoietin from hepatocytes promotes hematopoietic stem cell regeneration after myeloablation. *eLife* **10**, e69894 (2021).

49. Lee, Y., Leslie, J., Yang, Y. & Ding, L. Hepatic stellate and endothelial cells maintain hematopoietic stem cells in the developing liver. *J. Exp. Med.* **218**, e20200882 (2021).

50. Lee, Y., DiMaulo-Milk, E., Leslie, J. & Ding, L. Hematopoietic stem cells temporally transition to thrombopoietin dependence in the fetal liver. *Sci. Adv.* **8**, eabm7688 (2022).

51. Sarkaria, S. M. et al. Systematic dissection of coordinated stromal remodeling identifies Sox10(+) glial cells as a therapeutic target in myelofibrosis. *Cell Stem Cell* **30**, 832–850.e6 (2023).

52. Gao, L. snRNA-seq analysis LeiDingLab-Nature_Genetics_2023:v1. *Zenodo* https://doi.org/10.5281/zenodo.8280830 (2023).

Author contributions

H.H. performed all of the experiments. L.G. performed analysis on the snRNA-seq data. D.N.T. and G.V.-N. helped with the adipocyte culture experiments and editing of the manuscript. H.H. and L.D. designed the experiments, interpreted the results and wrote the manuscript.

Competing interests

The authors declare no competing interests.

Additional information

Extended data is available for this paper at https://doi.org/10.1038/s41588-023-01528-2.

Supplementary information The online version contains supplementary material available at https://doi.org/10.1038/s41588-023-01528-2.

**Correspondence and requests for materials** should be addressed to Lei Ding.

Peer review information *Nature Genetics* thanks the anonymous reviewers for their contribution to the peer review of this work. Peer reviewer reports are available.

Reprints and permissions information is available at www.nature.com/reprints.
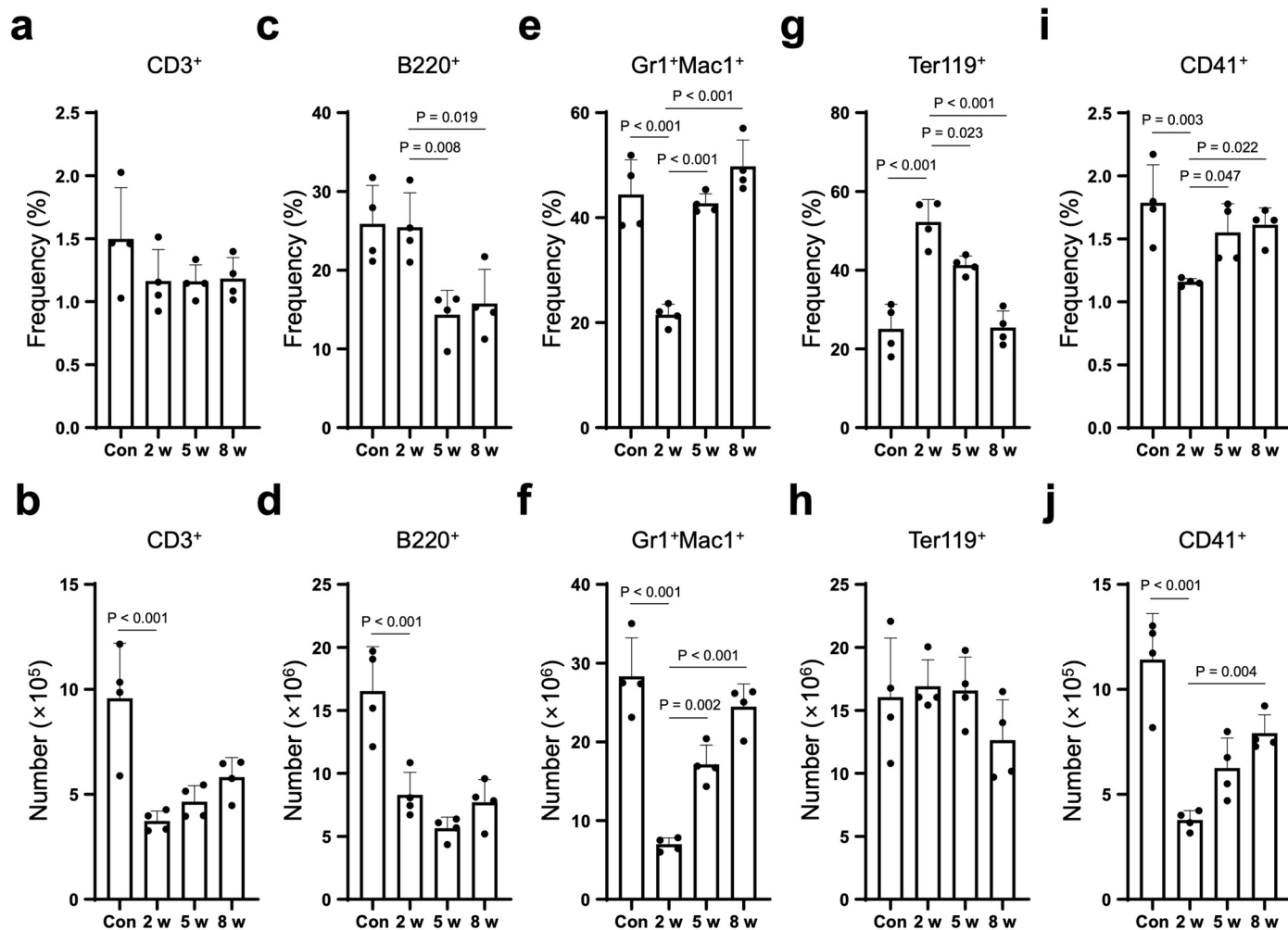
Extended Data Fig. 1 | Bone marrow regenerates after irradiation. a-j, Kinetics of maturing bone marrow hematopoietic cells after sublethal irradiation (6 Gy). Irradiated wild-type mice were analyzed at 2 weeks (2 w), 5 weeks (5 w), and 8 weeks (8 w) post-irradiation. Non-irradiated mice were used as controls (Con). The frequencies and numbers of CD3+ cells (a, b), B220+ cells (c, d), Gr1+ Mac1+ cells (e, f), Ter119+ cells (g, h), and CD41+ cells (i, j) are shown (n = 4 for each group). All data represent mean ± SD. One-way ANOVAs followed by Dunnett's test were used to assess statistical significance.
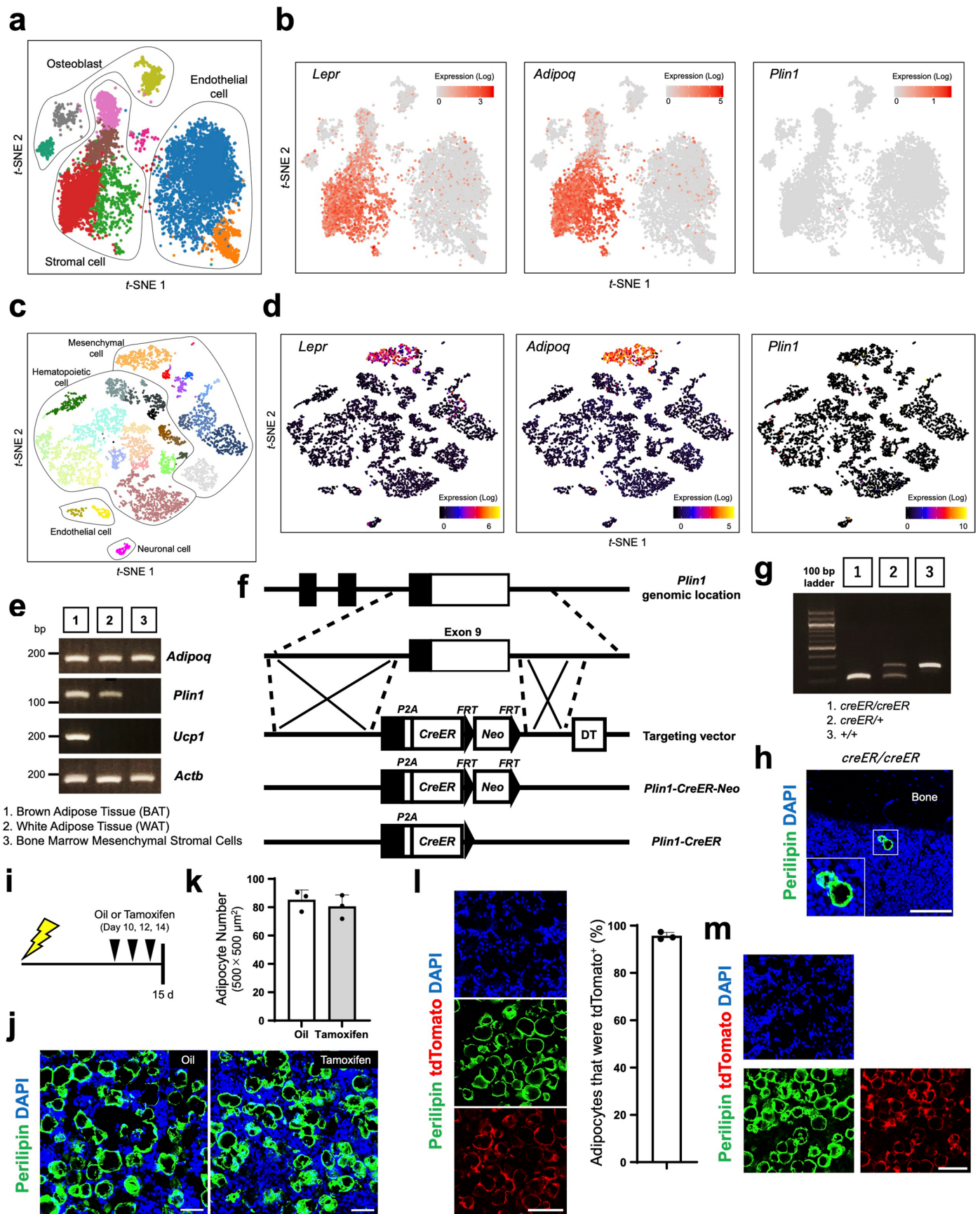
Extended Data Fig. 2 | See next page for caption.

Extended Data Fig. 2 | The generation of a *Plin1^creER^* knockin allele.
a, Clustering of bone marrow cells based on *t*-Distributed Stochastic Neighbor Embedding (*t*-SNE) from published data[12]. **b**, Gene expression levels of *Lepr*, *Adipoq*, and *Plin1* overlaid on *t*-SNE visualization. **c**, Clustering of bone marrow cells based on *t*-SNE from published data[11]. **d**, Gene expression levels of *Lepr*, *Adipoq*, and *Plin1* overlaid on *t*-SNE visualization. **e**, RT-PCR analyses revealed that *Plin1* is expressed by adipose tissues but not bone marrow mesenchymal stromal cells. *Adipoq* is expressed by bone marrow mesenchymal stromal cells while *Ucp1* is only expressed by brown adipose tissue. β-*Actin* was used as a control for RT-PCR. Lane 1: Brown Adipose Tissue (BAT), Lane 2: White Adipose Tissue (WAT), Lane 3: sorted CD45/Ter119/CD31⁻PDGFRα⁺ bone marrow mesenchymal stromal cells (n = 1). **f**, Gene targeting strategy. *Plin1^creER^* was generated by inserting *P2A-creER* into the ninth exon of *Plin1* using homologous recombination in ES cells. **g**, Representative genotyping PCR results confirmed the germline transmission of the *Plin1^creER^* allele (Lane 1: *creER/creER*, Lane 2: *creER/+*, Lane 3: +/+) (n = 3).
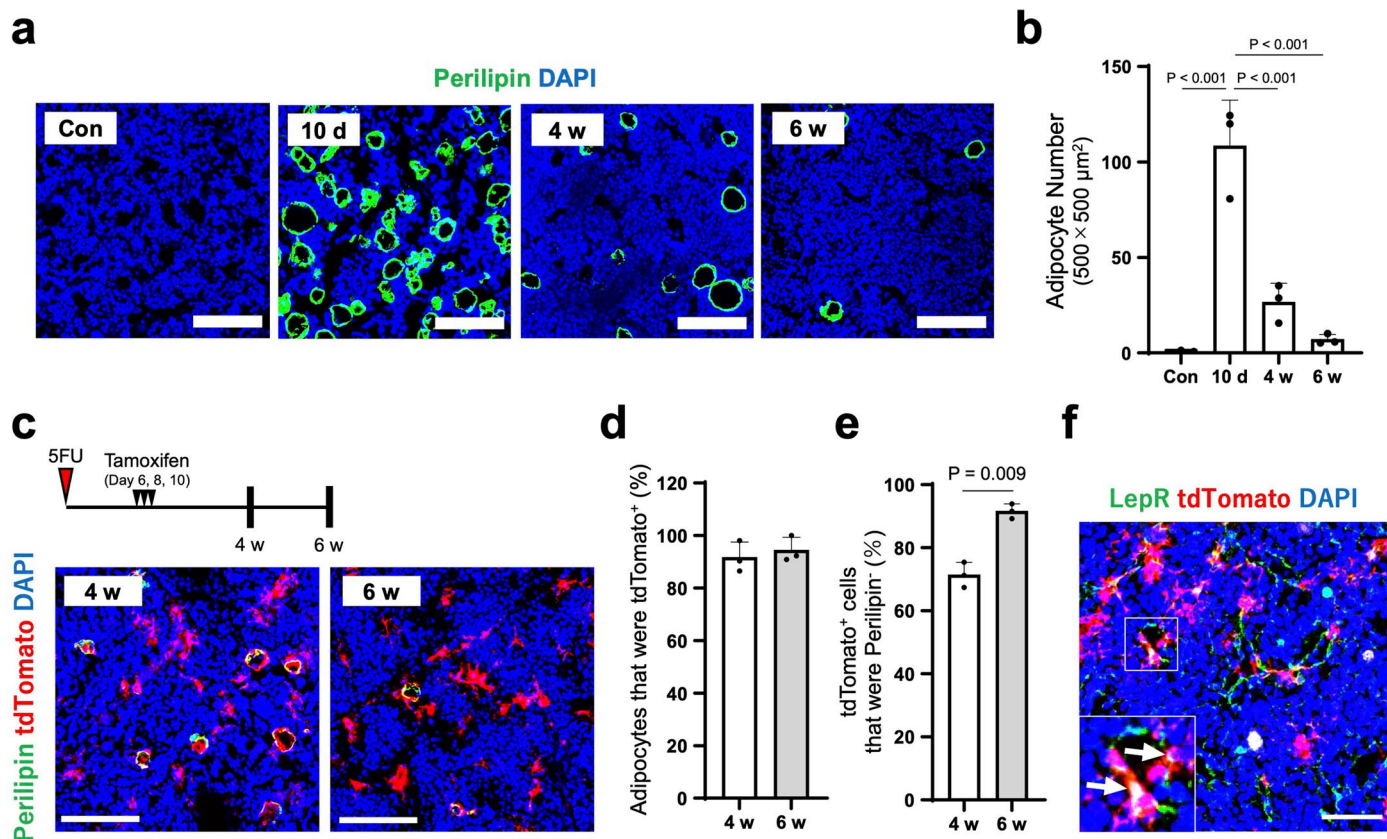
h, Representative image of the bone marrow from *creER/creER* homozygous mice (n = 2). Adipocytes were stained with an anti-perilipin antibody (in green). Nuclei were stained with DAPI (in blue). The square indicates an enlarged region. Scale bar, 100 μm. **i-k**, Sublethally irradiated (6 Gy) wild-type mice were treated with three doses of corn oil or tamoxifen on days 10, 12, and 14 and analyzed on day 15 post-irradiation. Experimental scheme (i). Representative images of the bone marrow (j). Quantification of bone marrow adipocytes stained with an anti-perilipin antibody (n = 3 for each group) (k). Scale bars, 50 μm. **l**, Representative whole-mount confocal images and frequency of perilipin⁺ adipocytes that were tdTomato⁺ (n = 3) in the bone marrow from *Plin1^creER^*; *Rosa26^LSL-tdTomato^* mice treated with tamoxifen on days 10, 12, and 14 and analyzed on day 15 post-irradiation. Scale bar, 100 μm. **m**, Individual channels of Fig. 2c (15 d). Scale bar, 100 μm. All data represent mean ± SD. A two-sided Student's t-test was used to assess statistical significance in k.
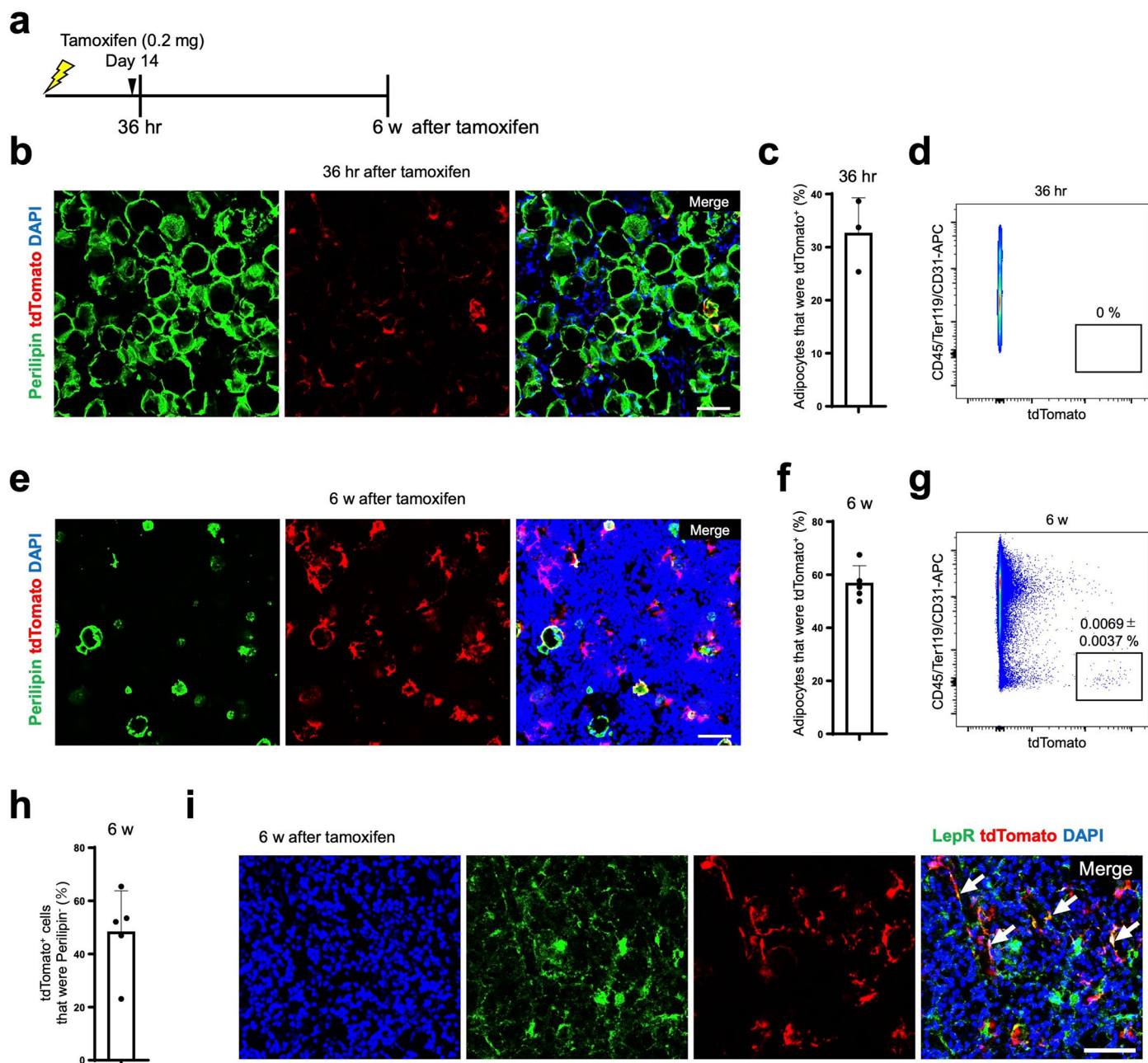
**Extended Data Fig. 3 | Prominent dedifferentiation of bone marrow adipocyte was evident with *Plin1-creER* induction by a low dose of tamoxifen.** **a**, Experimental scheme. **b**, **c**, Irradiated *Plin1^creER^;Rosa26^LSL-tdTomato^* mice were administered 0.2 mg tamoxifen on day 14 post-irradiation and analyzed 36 hours (36 hr) later (n = 3). Representative images of the bone marrow are shown. Scale bar, 50 μm. **d**, A representative flow cytometric plot showing no labeling of stromal cells in enzymatically digested bone marrow from irradiated *Plin1^creER^; Rosa26^LSL-tdTomato^* mice treated with 0.2 mg tamoxifen on day 14 post-irradiation and analyzed 36 hours (36 hr) later (n = 3). **e**, **f**, Irradiated *Plin1^creER^;Rosa26^LSL-tdTomato^* mice were administered 0.2 mg tamoxifen on day 14 and analyzed 6 weeks (6 w) later (n = 5). Representative images of the bone marrow are shown. Scale

bar, 50 μm. **g**, A representative flow cytometric plot of enzymatically digested bone marrow cells of the tibia from irradiated *Plin1^creER^;Rosa26^LSL-tdTomato^* mice treated as in e and f (n = 6). **h**, Frequency of tdTomato+ cells that were perilipin− in the bone marrow of irradiated *Plin1^creER^;Rosa26^LSL-tdTomato^* mice treated with 0.2 mg tamoxifen on day 14 post-irradiation and analyzed 6 weeks later (n = 5). **i**, Representative image showing adipocyte-derived tdTomato+ bone marrow stromal cells from irradiated *Plin1^creER^;Rosa26^LSL-tdTomato^* mice expressed LepR (arrows) (n = 2). The mice were treated with 0.2 mg tamoxifen on day 14 after irradiation and analyzed 6 weeks later. Scale bar, 50 μm. All data represent mean ± SD.

Extended Data Fig. 4 | Dedifferentiation of bone marrow adipocytes following 5FU challenge. a, Representative images of the bone marrow showing adipocyte content from the non⁻treated control (Con), 10 days (10 d), 4 weeks (4 w), or 6 weeks (6 w) after 5FU (150 mg kg⁻¹) administration in wild-type mice. Adipocytes were stained with an anti-perilipin antibody (in green). Scale bars, 100 µm. **b**, Quantification of bone marrow adipocytes following 5FU treatment (n = 3 for each group). **c-e**, *Plin1^creER*; *Rosa26^LSL-tdTomato* mice were treated with 3 doses of tamoxifen on days 6, 8, and 10 and analyzed 4 weeks (4 w) and 6 weeks (6 w) after 5FU treatment. Representative images of the bone marrow (c), the frequency of adipocytes that were tdTomato⁺ (n = 3 for each group) (d), and the frequency of tdTomato⁺ cells that were perilipin⁻ (n = 3 for each group) (e) are shown. Scale bars, 100 µm. **f**, Representative image showing that adipocyte-derived stromal cells express LepR (arrows) in the bone marrow from *Plin1^creER*; *Rosa26^LSL-tdTomato* mice after 5FU treatment (n = 3). The mice were treated with tamoxifen on days 6, 8, and 10, and analyzed 4 weeks after 5FU treatment. The square indicates an enlarged region. Scale bar, 50 µm. All data represent mean ± SD. A one-way ANOVA followed by Dunnett's test was used in b. Two-sided Student's t-tests were used in d and e.
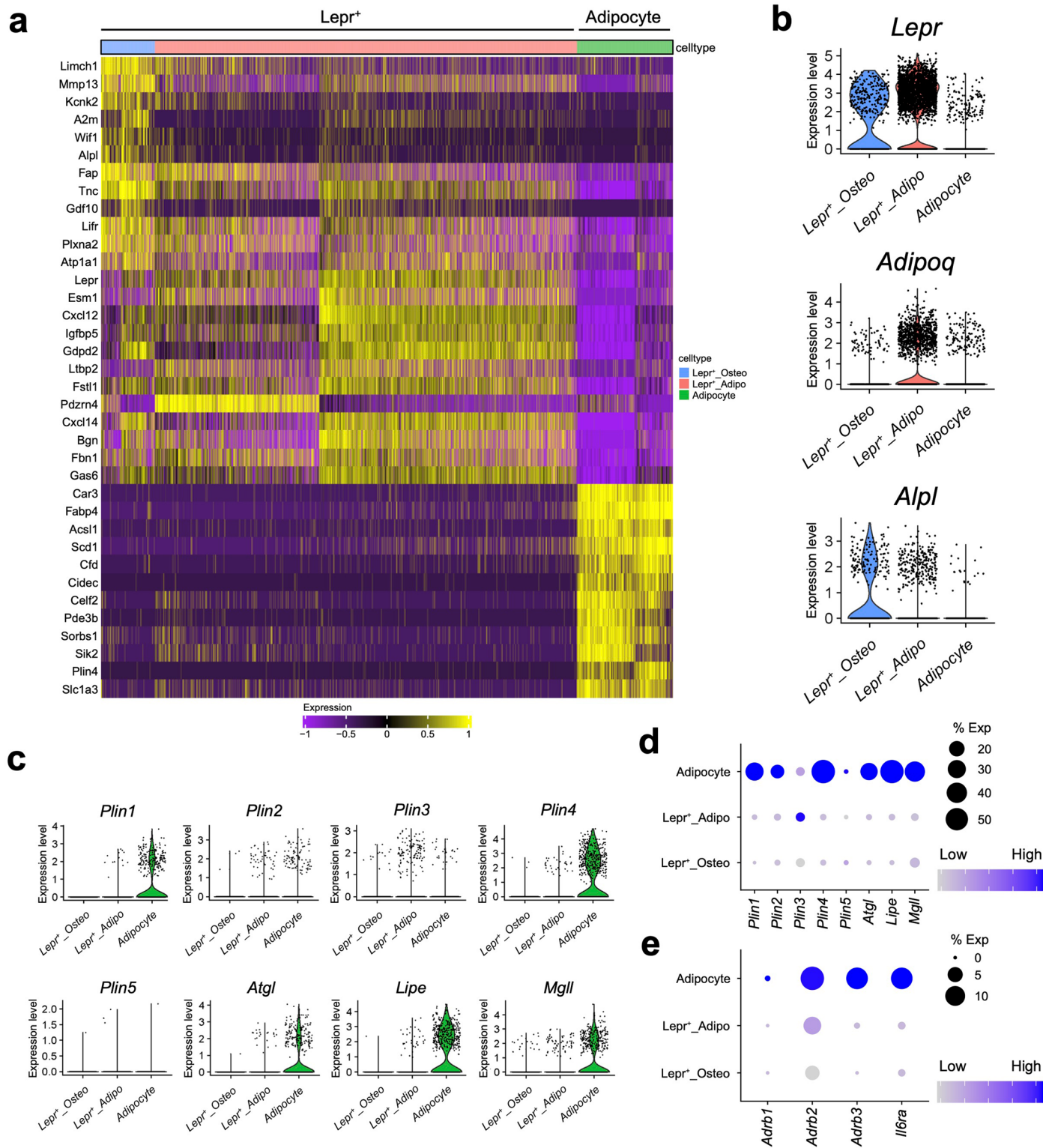
Extended Data Fig. 5 | snRNA-seq reveals stromal contribution by bone marrow adipocytes during regeneration. a, Heatmap showing the signature genes of two distinct mesenchymal cell clusters in the regenerating bone marrow (Lepr[+] and Adipocyte). The Lepr[+] cluster is further divided into two clusters (Lepr[+]_Osteo and Lepr[+]_Adipo). **b**, Violin plots showing the expression levels of *Lepr*, *Adipoq*, and *Alpl*. **c**, **d**, Expression levels of Perilipin family genes (*Plin1*, *Plin2*, *Plin3*, *Plin4*, and *Plin5*) and three genes coding lipases (*Atgl*, *Lipe*, and *Mgll*) are shown in violin plots (c) and dot plot (d). **e**, Dot plot showing the expression levels of *Adrb1*, *Adrb2*, *Adrb3*, and *Il6ra*.
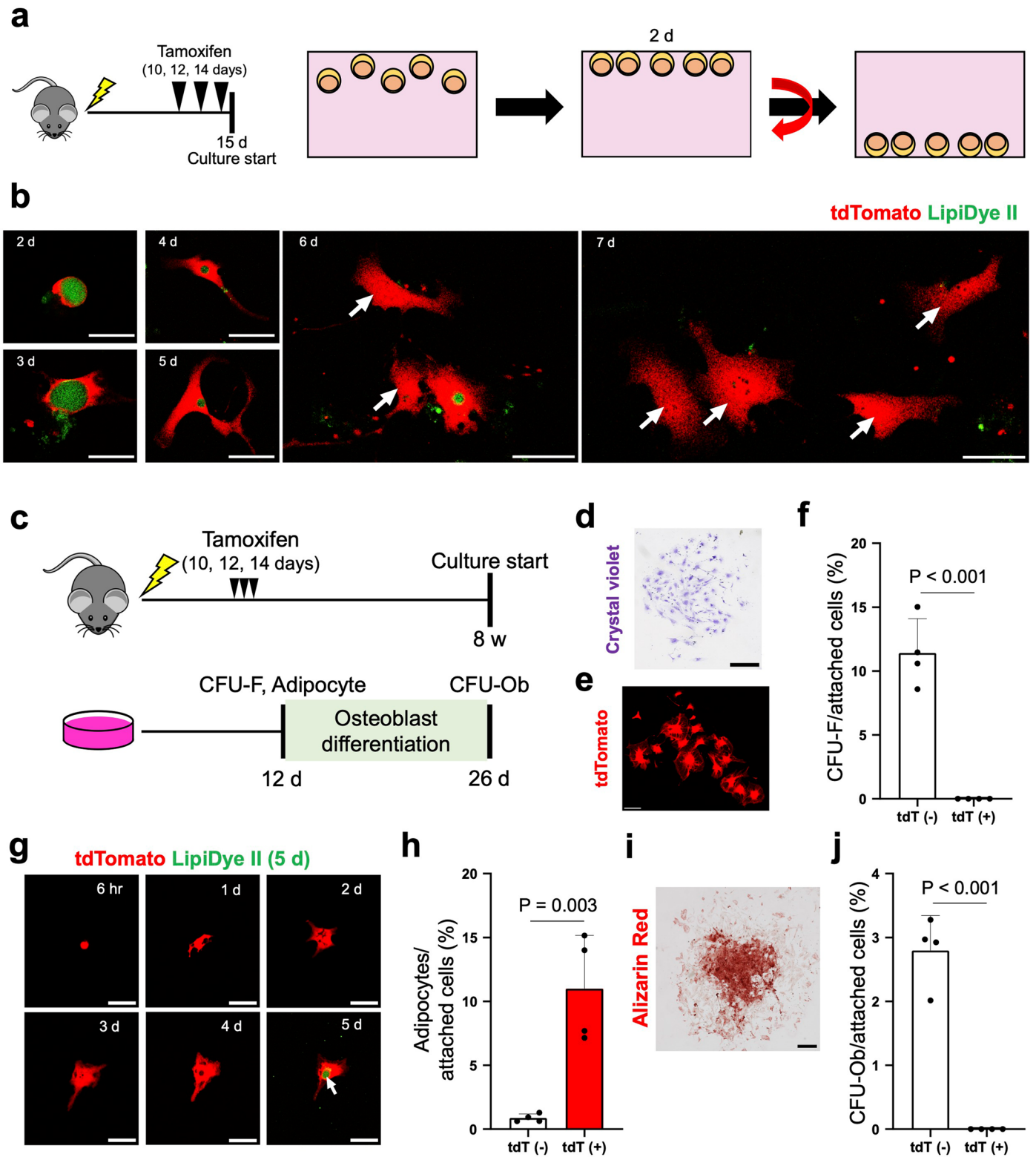
Extended Data Fig. 6 | See next page for caption.

Extended Data Fig. 6 | Ex vivo properties of mature bone marrow adipocytes and their derivatives. a, Experimental scheme for monitoring bone marrow adipocyte culture in vitro. Individual bone marrow adipocytes isolated from *Plin1^creER^;Rosa26^LSL-tdTomato^* mice at 15 days after sublethal irradiation (tamoxifen administration on day 14) were followed by time-lapse imaging in culture for 7 days. Lipid-filled adipocytes adhering to the ceiling of the flask on day 2 were tracked by confocal microscopy. **b**, Representative images of live cell imaging of bone marrow tdTomato⁺ adipocytes and their derivatives from day 2 to 7 (n = 2). Arrows point to adipocyte-derived cells (tdTomato⁺) with a stromal morphology but lacking lipid droplets (LipiDye II negative). Lipid droplets were stained with LipiDye II (in green). Scale bars, 50 μm. **c**, Experimental scheme for testing stromal cell function in vitro. **d**, Sublethally irradiated *Plin1^creER^;Rosa26^LSL-tdTomato^* mice were administered tamoxifen on days 10, 12, and 14 post-irradiation. At 8 weeks post-irradiation, CFU-F assays were performed with enzymatically digested bone marrow cells. Attached cells at clonal density were counted one day after plating and colonies were counted 12 days later. A representative image of a CFU-F colony (>25 cells) stained by Crystal Violet is shown. Scale bar, 500 μm.

e, A representative image showing that tdTomato⁺ stromal cells are proliferative. The cells were from single tdTomato⁺ cells. Scale bar, 200 μm. **f**, Quantifications of CFU-F frequency from attached tdTomato⁻ and tdTomato⁺ stromal cells (n = 4). **g**, Representative images of live cell imaging of a single tdTomato⁺ cell for 5 days. Lipid droplets were stained by LipiDye II (in green, arrow) on day 5 to show that lipid droplets are accumulating in a tdTomato⁺ cell. Scale bars, 50 μm. **h**, Quantification of adipocyte frequency from attached tdTomato⁻ and tdTomato⁺ stromal cells (n = 4). After initiation of cell culture as in c, cells were cultured in a normal media without differentiation induction for 12 days and then LipiDye II⁺ adipocytes were counted. **i**, A representative image of a colony stained by Alizarin Red S showing osteoblastic differentiation. Scale bar, 500 μm. **j**, Quantification of CFU-osteoblasts (CFU-Ob) frequency from attached tdTomato⁻ and tdTomato⁺ stromal cells (n = 4). After initiation of cell culture as in c, cells were cultured in a normal media for 12 days and then cultured in osteolineage differentiation media for 14 days. All data represent mean ± SD. Two-sided Student's t-tests were used to assess statistical significance.
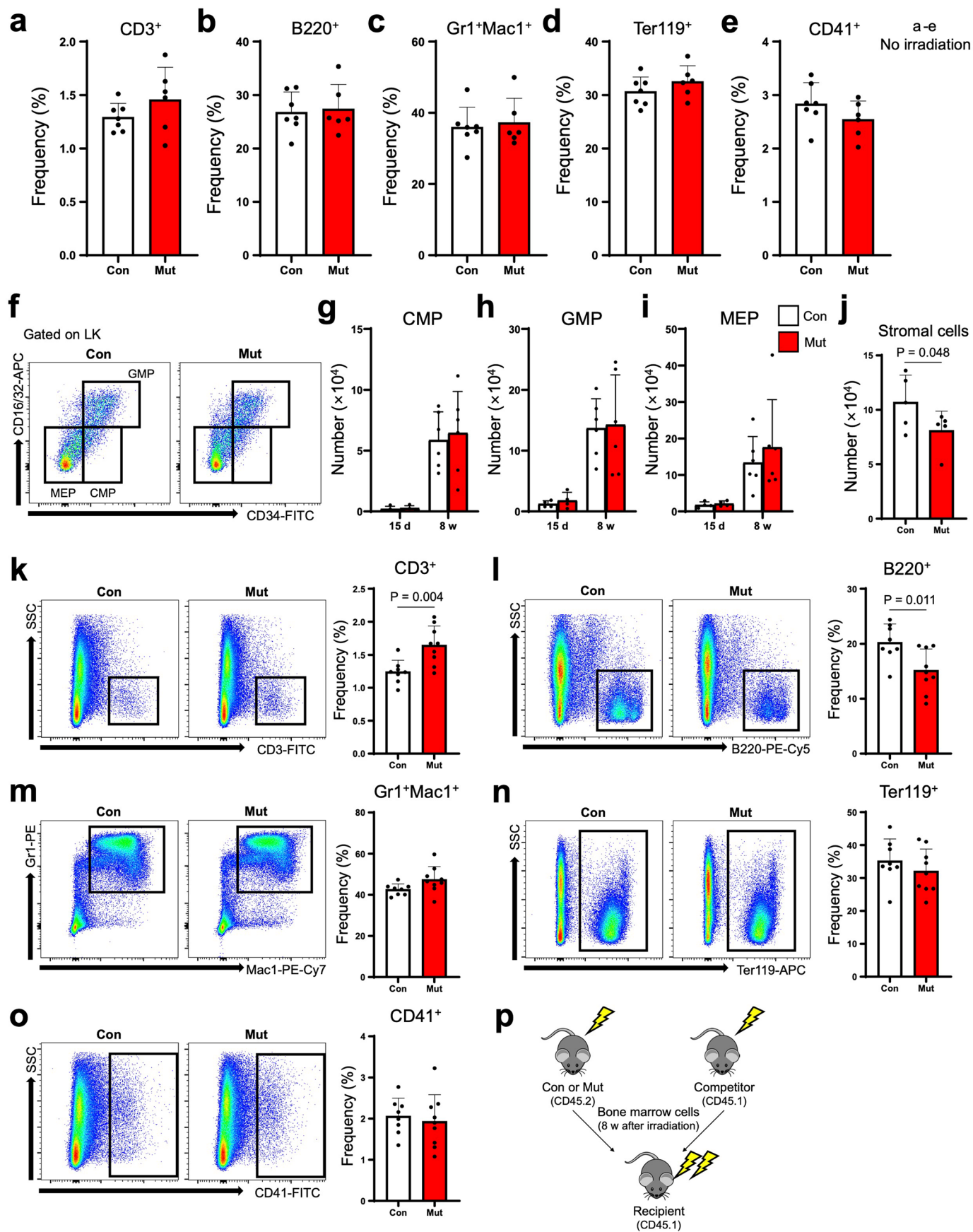
Extended Data Fig. 7 | See next page for caption.

Extended Data Fig. 7 | Perturbed lymphopoiesis in the bone marrow of *Prx1-cre; Atgl*^{fl/fl} mice after irradiation. a-e, The frequencies and numbers of CD3⁺ cells (a), B220⁺ cells (b), Gr1⁺ Mac1⁺ cells (c), Ter119⁺ cells (d) and CD41⁺ cells (e) in the bone marrow of *Prx1-cre; Atgl*^{fl/fl} (Mut) and control mice (Con) (n = 7 for Con, n = 6 for Mut). **f-i**, Representative flow cytometric plots of LK (Lin[−] c-Kit⁺) cells from *Prx1^{−}cre; Atgl*^{fl/fl} (Mut) and control mice (Con) at 8 weeks post-irradiation (f). Quantifications of CMP number (g), GMP number (h), and MEP number (i) in the bone marrow of Mut and Con at 15 days (n = 4 for each group) and 8 weeks (n = 6 for each group) post-irradiation. **j**, The number of CD45/Ter119/ CD31^{−}PDGFRα⁺ bone marrow mesenchymal stromal cells of *Prx1^{−}cre; Atgl*^{fl/fl} (Mut) and control mice (Con) at 8 weeks post-irradiation (n = 5 for each group).

A one-sided Student's t-test was used. **k-o**, Representative flow cytometric plots and frequencies of bone marrow cells that are positive for CD3 (k), B220 (l), Gr1 and Mac1 (m), Ter119 (n), and CD41 (o). *Prx1-cre; Atgl*^{fl/fl} (Mut) and control mice (Con) were analyzed at 8 weeks post-irradiation (n = 8 for Con, n = 9 for Mut). **p**, Experimental scheme for transplantation assays in Fig. 7m. Competitive transplantation of 10⁶ bone marrow cells (CD45.2) from *Prx1-cre; Atgl*^{fl/f} or control mice with 10⁶ competitor bone marrow cells (CD45.1) into lethally irradiated recipients. Donor and competitor cells were harvested from sublethally irradiated mice at 8 weeks post-irradiation. All data represent mean ± SD. Two-sided Student's t-tests were used in a-e, g-i, and k-o.

nature portfolio

Corresponding author(s): Lei Ding

Last updated by author(s): Aug 9, 2023

Reporting Summary

Nature Portfolio wishes to improve the reproducibility of the work that we publish. This form provides structure for consistency and transparency in reporting. For further information on Nature Portfolio policies, see our Editorial Policies and the Editorial Policy Checklist.

Statistics

For all statistical analyses, confirm that the following items are present in the figure legend, table legend, main text, or Methods section.

n/a	Confirmed	
☐	☒	The exact sample size (*n*) for each experimental group/condition, given as a discrete number and unit of measurement
☐	☒	A statement on whether measurements were taken from distinct samples or whether the same sample was measured repeatedly
☐	☒	The statistical test(s) used AND whether they are one- or two-sided *Only common tests should be described solely by name; describe more complex techniques in the Methods section.*
☐	☒	A description of all covariates tested
☐	☒	A description of any assumptions or corrections, such as tests of normality and adjustment for multiple comparisons
☐	☒	A full description of the statistical parameters including central tendency (e.g. means) or other basic estimates (e.g. regression coefficient) AND variation (e.g. standard deviation) or associated estimates of uncertainty (e.g. confidence intervals)
☐	☒	For null hypothesis testing, the test statistic (e.g. *F*, *t*, *r*) with confidence intervals, effect sizes, degrees of freedom and *P* value noted *Give P values as exact values whenever suitable.*
☒	☐	For Bayesian analysis, information on the choice of priors and Markov chain Monte Carlo settings
☒	☐	For hierarchical and complex designs, identification of the appropriate level for tests and full reporting of outcomes
☒	☐	Estimates of effect sizes (e.g. Cohen's *d*, Pearson's *r*), indicating how they were calculated

Our web collection on statistics for biologists contains articles on many of the points above.

Software and code

Policy information about availability of computer code

Data collection	FACSDiva (v9), Leica Application Suite X (v3.5.7.23225), BioRad CFX Manager (v3.1), Illumina Basespace.
Data analysis	Flowjo (v10.8.1), FACSDiva (v9), Graphpad Prism (v6.3.1), Excel (2019), Seurat (v4.2.0), CellBender (v0.2.2), Scillus (v0.5.0), DoubleFinder (v2.0.3), ScProportionTest (v0.0.0.9000)

For manuscripts utilizing custom algorithms or software that are central to the research but not yet described in published literature, software must be made available to editors and reviewers. We strongly encourage code deposition in a community repository (e.g. GitHub). See the Nature Portfolio guidelines for submitting code & software for further information.

Data

Policy information about availability of data

All manuscripts must include a data availability statement. This statement should provide the following information, where applicable:
- Accession codes, unique identifiers, or web links for publicly available datasets
- A description of any restrictions on data availability
- For clinical datasets or third party data, please ensure that the statement adheres to our policy

RNA-seq data generated in this study have been deposited at GEO under accession number GSE227255. Previously published scRNA-seq data were used in this study: GSE108892 (https://aifantislab.com/niche/) and GSE122467 (https://apps.embl.de/nicheview/). All data are publicly available.

Human research participants

Reporting on sex and gender	NA
Population characteristics	NA
Recruitment	NA
Ethics oversight	NA

Note that full information on the approval of the study protocol must also be provided in the manuscript.

Field-specific reporting

Please select the one below that is the best fit for your research. If you are not sure, read the appropriate sections before making your selection.

☒ Life sciences   ☐ Behavioural & social sciences   ☐ Ecological, evolutionary & environmental sciences

For a reference copy of the document with all sections, see nature.com/documents/nr-reporting-summary-flat.pdf

Life sciences study design

All studies must disclose on these points even when the disclosure is negative.

Sample size	Sample sizes were not based on power calculations. They were based on prior research experiences for similar assays.
Data exclusions	No data were excluded.
Replication	All experiments with quantification data were repeated with at least three independent biological replicates in independent experiments. All replications were successful, with similar results.
Randomization	Mice with desired genotypes/treatments were randomly chosen for analysis.
Blinding	The investigators were not blinded to allocation during experiments and outcome assessment.

Reporting for specific materials, systems and methods

We require information from authors about some types of materials, experimental systems and methods used in many studies. Here, indicate whether each material, system or method listed is relevant to your study. If you are not sure if a list item applies to your research, read the appropriate section before selecting a response.

Materials & experimental systems

n/a	Involved in the study
☐	☒ Antibodies
☒	☐ Eukaryotic cell lines
☒	☐ Palaeontology and archaeology
☐	☒ Animals and other organisms
☒	☐ Clinical data
☒	☐ Dual use research of concern

Methods

n/a	Involved in the study
☒	☐ ChIP-seq
☐	☒ Flow cytometry
☒	☐ MRI-based neuroimaging

Antibodies

Antibodies used	For flow cytometry CD45-APC (30-F11, 103112, BioLegend) Ter119-APC (TER-119, 116212, BioLegend) Ter119-FITC (TER-119, 116206, BioLegend) Ter119-PE (TER-119, 116208, BioLegend) CD31-APC (390, 102410, BioLegend) B220-FITC (6B2, 103206, BioLegend)

B220-PE (6B2, 103208, BioLegend)
B220-PE-Cy5 (6B2, 103210, BioLegend)
Gr1-FITC (8C5, 108406, BioLegend)
Gr1-PE (8C5, 108408, BioLegend)
Gr1-PE-Cy7 (8C5, 108416, BioLegend)
CD2-FITC (RM2-5, 100105, BioLegend)
CD2-PE (RM2-5, 100108, BioLegend)
CD3-FITC (17A2, 100204, BioLengend)
CD3-PE (17A2, 100206, BioLengend)
CD5-FITC (53-7.3, 100606, BioLegend)
CD5-PE (53-7.3, 100608, BioLegend)
CD8-FITC (53-6.7, 100706, BioLegend)
CD8-PE (53-6.7, 100708, BioLegend)
CD150-PE (TC15-12F12.2, 115904, BioLegend)
CD48-APC (HM48-1, 103412, BioLegend)
Sca-1-PE-Cy7 (E13-161.7, 108114, BioLegend)
Sca-1-Alexa Fluor 700 (D7, 108142, BioLegend)
c-Kit-APC-Cy7 (2B8, 105826, BioLegend)
Flt3 (CD135)-PE-Cy5 (A2F10, 135312, BioLegend)
CD16/32-APC (93, 101326, BioLegend)
CD127-biotin (A7R34, 135006, BioLegend)
CD34-FITC (RAM34, 560238, BD Biosciences)
Mac1 (Cd11b)-PE-Cy7 (M1/70, 101216, BioLegend)
CD41-FITC (MWReg30, 133904, BioLegend)
CD140a-PE-Cy7 (APA5, 135912, BioLegend)
CD140a-biotin (APA5, 135910, BioLegend)
CXCL12-FITC (79018, IC350F, R&D)
Mouse IgG1-FITC (MOPC-21, 400107, BioLegend)
CD45.2-FITC (104, 109806, BioLegend)
CD45.1-APC-Cy7 (A20, 110716, BioLegend)

For immunostaining
Rabbit-anti-Perilipin-1 (D1D8, 9349S, Cell Signaling)
Goat-anti-LepR (AF497, R&D)
Goat-anti-IL7 (AF407, R&D)
Cleaved Caspase-3- Alexa Fluor-488 (Asp175, 9669S, Cell Signaling)

Validation

They are all from commercial sources (Biolegend, BD Biosciences, Cellsignaling or R&D) and are widely used in the field.

Validation for all antibodies is available at the vendor's website.
For flow cytometry
CD45-APC (30-F11, 103112, BioLegend) https://www.biolegend.com/en-us/products/apc-anti-mouse-cd45-antibody-97
Ter119-APC (TER-119, 116212, BioLegend) https://www.biolegend.com/en-us/products/apc-anti-mouse-ter-119-erythroid-cells-antibody-1863
Ter119-FITC (TER-119, 116206, BioLegend) https://punchout.biolegend.com/de-de/products/fitc-anti-mouse-ter-119-erythroid-cells-antibody-1865
Ter119-PE (TER-119, 116208, BioLegend) https://www.biolegend.com/en-us/products/pe-anti-mouse-ter-119-erythroid-cells-antibody-1867
CD31-APC (390, 102410, BioLegend) https://www.biolegend.com/en-us/products/apc-anti-mouse-cd31-antibody-118
B220-FITC (6B2, 103206, BioLegend) https://www.biolegend.com/de-at/products/fitc-anti-mouse-human-cd45r-b220-antibody-445
B220-PE (6B2, 103208, BioLegend) https://www.biolegend.com/ja-jp/clone-search/pe-anti-mouse-human-cd45r-b220-antibody-447
B220-PE-Cy5 (6B2, 103210, BioLegend) https://www.biolegend.com/en-us/products/pe-cyanine5-anti-mouse-human-cd45r-b220-antibody-448
Gr1-FITC (8C5, 108406, BioLegend) https://www.biolegend.com/de-de/soluble-mhc/fitc-anti-mouse-ly-6g-ly-6c-gr-1-antibody-458
Gr1-PE (8C5, 108408, BioLegend) https://www.biolegend.com/nl-nl/products/pe-anti-mouse-ly-6g-ly-6c-gr-1-antibody-460
Gr1-PE-Cy7 (8C5, 108416, BioLegend) https://www.biolegend.com/en-us/products/pe-cyanine7-anti-mouse-ly-6g-ly-6c-gr-1-antibody-1931
CD2-FITC (RM2-5, 100105, BioLegend) https://www.biolegend.com/en-us/global-elements/pdf-popup/fitc-anti-mouse-cd2-antibody-472
CD2-PE (RM2-5, 100108, BioLegend) https://www.biolegend.com/en-ie/products/pe-anti-mouse-cd2-antibody-473
CD3-FITC (17A2, 100204, BioLengend) https://www.biolegend.com/en-us/products/fitc-anti-mouse-cd3-antibody-45
CD3-PE (17A2, 100206, BioLengend) https://www.biolegend.com/ja-jp/products/pe-anti-mouse-cd3-antibody-47
CD5-FITC (53-7.3, 100606, BioLegend) https://www.biolegend.com/en-us/products/fitc-anti-mouse-cd5-antibody-159
CD5-PE (53-7.3, 100608, BioLegend) https://www.biolegend.com/en-us/products/pe-anti-mouse-cd5-antibody-160
CD8-FITC (53-6.7, 100706, BioLegend) https://www.biolegend.com/de-at/cell-health/fitc-anti-mouse-cd8a-antibody-153
CD8-PE (53-6.7, 100708, BioLegend) https://www.biolegend.com/nl-nl/clone-search/pe-anti-mouse-cd8a-antibody-155
CD150-PE (TC15-12F12.2, 115904, BioLegend) https://www.biolegend.com/fr-lu/clone-search/pe-anti-mouse-cd150-slam-antibody-1369
CD48-APC (HM48-1, 103412, BioLegend) https://www.biolegend.com/en-us/products/apc-anti-mouse-cd48-antibody-3622
Sca-1-PE-Cy7 (E13-161.7, 108114, BioLegend) https://www.biolegend.com/en-us/products/pe-cyanine7-anti-mouse-ly-6a-e-sca-1-antibody-3137
Sca-1-Alexa Fluor 700 (D7, 108142, BioLegend) https://www.biolegend.com/ja-jp/products/alexa-fluor-700-anti-mouse-ly-6a-e-sca-1-antibody-12078
c-Kit-APC-Cy7 (2B8, 105826, BioLegend) https://www.biolegend.com/en-us/products/apc-cyanine7-anti-mouse-cd117-c-kit-antibody-5905

Flt3 (CD135)-PE-Cy5 (A2F10, 135312, BioLegend) https://www.biolegend.com/en-gb/soluble-mhc/pe-cyanine5-anti-mouse-cd135-antibody-6300
CD16/32-APC (93, 101326, BioLegend) https://www.biolegend.com/en-gb/products/apc-anti-mouse-cd16-32-antibody-6282
CD127-biotin (A7R34, 135006, BioLegend) https://www.biolegend.com/ja-jp/products/biotin-anti-mouse-cd127-il-7ralpha-antibody-6269
CD34-FITC (RAM34, 560238, BD Biosciences) https://www.bdbiosciences.com/en-us/products/reagents/flow-cytometry-reagents/research-reagents/single-color-antibodies-ruo/fitc-rat-anti-mouse-cd34.560238
Mac1 (Cd11b)-PE-Cy7 (M1/70, 101216, BioLegend) https://www.biolegend.com/en-us/products/pe-cyanine7-anti-mouse-human-cd11b-antibody-1921
CD41-FITC (MWReg30, 133904, BioLegend) https://www.biolegend.com/en-us/search-results/fitc-anti-mouse-cd41-antibody-5896
CD140a-PE-Cy7 (APA5, 135912, BioLegend) https://www.biolegend.com/en-us/explore-new-products/pe-cyanine7-anti-mouse-cd140a-antibody-14822
CD140a-biotin (APA5, 135910, BioLegend) https://www.biolegend.com/en-us/products/biotin-anti-mouse-cd140a-antibody-6440
CXCL12-FITC (79018, IC350F, R&D) https://www.rndsystems.com/products/human-mouse-cxcl12-sdf-1-fluorescein-conjugated-antibody-79018_ic350f
Mouse IgG1-FITC (MOPC-21, 400107, BioLegend) https://www.biolegend.com/en-us/products/fitc-mouse-igg1-kappa-isotype-ctrl-1406
CD45.2-FITC (104, 109806, BioLegend) https://www.biolegend.com/en-us/products/fitc-anti-mouse-cd45-2-antibody-6
CD45.1-APC-Cy7 (A20, 110716, BioLegend) https://www.biolegend.com/en-us/products/apc-cyanine7-anti-mouse-cd45-1-antibody-2320

For immunostaining
Rabbit-anti-Perilipin-1 (D1D8, 9349S, Cell Signaling) https://www.cellsignal.com/products/primary-antibodies/perilipin-1-d1d8-xp-rabbit-mab/9349
Goat-anti-LepR (AF497, R&D) https://www.rndsystems.com/products/mouse-leptin-r-antibody_af497
Goat-anti-IL7 (AF407, R&D) https://www.rndsystems.com/products/mouse-il-7-antibody_af407
Cleaved Caspase-3- Alexa Fluor-488 (Asp175, 9669S, Cell Signaling) https://www.cellsignal.com/products/antibody-conjugates/cleaved-caspase-3-asp175-antibody-alexa-fluor-488-conjugate/9669

Animals and other research organisms

Policy information about studies involving animals; ARRIVE guidelines recommended for reporting animal research, and Sex and Gender in Research

Laboratory animals	Young adult (8-10 weeks old) Prx1-cre, Rosa26-LsL-tdTomato, Col2.3-GFP, Pdgfra-GFP, Atgl-fl, and Plin1-creER mice were used. They are maintained on B6 background.
Wild animals	No wild animals were used in the study.
Reporting on sex	Both males and females were included for analysis.
Field-collected samples	No field-collected samples were used in the study.
Ethics oversight	All protocols were approved by Columbia University Committee on the Institute Animal Care and Use.

Note that full information on the approval of the study protocol must also be provided in the manuscript.

Flow Cytometry

Plots

Confirm that:

☒ The axis labels state the marker and fluorochrome used (e.g. CD4-FITC).

☒ The axis scales are clearly visible. Include numbers along axes only for bottom left plot of group (a 'group' is an analysis of identical markers).

☒ All plots are contour plots with outliers or pseudocolor plots.

☒ A numerical value for number of cells or percentage (with statistics) is provided.

Methodology

Sample preparation	For analyzing hematopoietic cells, bone marrow cells were isolated by flushing long bones (femur and tibia). The cells were passed through 25G syringes with Ca2+ and Mg2+ free HBSS with 2% heat-inactivated bovine serum for single cell suspension. Then cells were filtered through 70 um nylon mesh. For analyzing and sorting stromal cells, bone marrow was flashed by centrifuge (5000 g, 1 sec, RT) and followed by digesting with Collagenase I (1 mg ml−1), Collagenase IV (200 U ml−1) and DNase I (200 U ml−1) at 37 degrees for 20 min. Then cells were filtered through 70 um nylon mesh.
Instrument	Samples were run on FACSAria II, BD LSR II, or FACSCelesta flow cytometers.
Software	FACSDiva (BD) or FlowJo (Tree Star) software were used for data analysis.

Cell population abundance	The HSC frequency is about 0.007% in wild type bone marrow. Stromal cell frequency is about 0.01-0.04% in the bone marrow. We routinely collect 1 million bone marrow cells for analysis.
Gating strategy	The gating strategy is illustrated in the figures. Positivity is defined by single color stained controls and comparing with no staining or Isotype staining controls.

☒ Tick this box to confirm that a figure exemplifying the gating strategy is provided in the Supplementary Information.